Model calculations of phase diagrams of magnetic alloys on the body-centered-cubic lattice

Burkhard Dünweg and Kurt Binder
Institut für Physik, Johannes Gutenberg-Universität Mainz, D-6500 Mainz, Postfach 3980, Federal Republic of Germany
(Received 10 April 1987)

A comparative study of a model of binary (AB) alloys on the body-centered-cubic lattice, one species (A) being magnetic and the other (B) being nonmagnetic, is presented. Allowing for nearest-neighbor and next-nearest-neighbor interactions as well as nearest-neighbor magnetic-exchange interactions, a variety of phases occurs as is familiar from the Fe-Al phase diagram: both paramagnetic and ferromagnetic $A2(\alpha)$, $B2$(Fe-Al), and DO_3(Fe_3Al) phases, with order-disorder phase transitions as well as transitions between different ordered phases; some of these transitions being of second order and some of first order. The statistical mechanics of the model is treated both by the molecular-field approximation, the Kikuchi cluster-variation method in the tetrahedron approximation, and the Monte Carlo method. We find that the molecular-field approximation yields a qualitatively wrong phase diagram which substantially overestimates the stability of the ordered phases, in contrast to previous work suggesting that it yields a reliable description of the Fe-Al problem. On the other hand, the cluster-variation phase diagram is in rather close agreement with the (presumably most accurate) Monte Carlo results, the transition temperatures being too high by only a few percent. It is shown that the crystallographic order induces a staggered magnetization in the ferromagnetic $B2$ and DO_3 phases. Consequences for work on related problems and experiments are briefly discussed.

I. INTRODUCTION

The calculation of phase diagrams for simple models of metallic alloys has been a problem of long-standing interest (see Refs. 1–3 for recent reviews). Assuming an Ising-model–type description where each lattice site of a given lattice [face-centered-cubic (fcc), body-centered-cubic (bcc), etc.] can either be taken by an A atom or a B atom and suitable model assumptions for the (short-range) effective interaction, the problem is a task of statistical mechanics. Since an exact solution is not at hand, approximate or numerical methods must be used. Apart from its interest in statistical mechanics itself, this problem is of practical interest in metallurgy: If for a particular alloy suitable effective interactions are known, and the approximate method used for theoretical predictions is reliable, one can predict order parameters referring to both long- and short-range order in various parts of the phase diagram, predict the small-angle scattering intensity, etc. Conversely, a comparison of such predictions to experimental data may lead to a refined understanding of the fundamental effective interactions in the alloy.

A crucial point of such comparisons, however, is to establish that the approximate method used for theoretical predictions is accurate enough: otherwise the comparison is meaningless. Motivated by the prototypic example of the Au-Cu phase diagram, a lot of work has been devoted to the fcc Ising lattice including only nearest-neighbor[1–18] or also next-nearest neighbor[2,11–13,19–23] (and sometimes nonpairwise[24,25]) interactions. The general consensus is that the Bragg-Williams mean-field approximation[4,5] is not at all quantitatively reliable, it often yields a qualitatively incorrect phase diagram. On the other hand, the Kikuchi[26] cluster-variation method in the tetrahedron approximation[7,19] already performs much better: Typically it overestimates transition temperatures by about 5%, apart from the vicinity of the triple point in the nearest-neighbor fcc model where the error is much larger, but due to the "frustration"[27] of the model this case clearly is exceptional (and still not fully understood[9–18]).

Much less work has been devoted to other lattices. The bcc lattice with nearest-neighbor interactions has been studied both by mean-field theory,[28] and cluster-variation[29] and Monte Carlo[30] methods, but this case is less interesting since only a single second-order transition from the disordered ($A2$) structure to the ordered ($B2$) structure occurs (Fig. 1). The Bragg-Williams mean-field[28] and the cluster-variation[29] approximations have been applied to models with interactions to further neighbors, allowing the occurrence of the DO_3 phase (Fig. 1); also, magnetic degrees of freedom have been incorporated into Bragg-Williams calculations.[31,32] Some of these attempt to model the Fe-Al phase diagram.[32] However, although interaction parameters are found[32] such that the mean-field phase diagram roughly matches the experimental phase diagram of Fe-Al alloys,[33] we feel that this agreement is merely accidental: There is no reason to expect that the Bragg-Williams approximation will yield a quantitatively reliable phase diagram for any lattice. This conclusion will be substantiated in the present paper, where a comparative study of a model with both nearest- and next-nearest-neighbor interactions, and including a magnetic degree of freedom, is studied by the Bragg-Williams method, the cluster-variation method, and the Monte Carlo method. Our study, however, does not attempt to explain the real Fe-

 ©1987 The American Physical Society

Al system: Due to the itinerant character of the electrons responsible for the magnetic properties of Fe, a realistic theory for this alloy as yet is impossible. Our model of a binary alloy with one species being magnetic disregards any realistic account of electronic structure: We simply model the magnetic degree of freedom by an Ising spin $\sigma = \pm 1$. While the Monte Carlo method could also easily be applied to a model with localized classical spins (Heisenberg model with $\sigma \to \infty$),[34] the choice of discrete Ising spins allows a rather straightforward application of the cluster-variation method too.

The outline of this paper is as follows. In Sec. II we define the model, describe the structures and the order parameters which are calculated, and summarize the exact information on ground-state properties (following Kanamori[35]). Sections III and IV summarize the mean-field and cluster-variation methods, as used in our work (more details can be found in Ref. 36). Section V describes our Monte Carlo results and compares them to the cluster-variation results; low-temperature properties are also compared to exact low-temperature expansions. Finally, Sec. VI summarizes our conclusions.

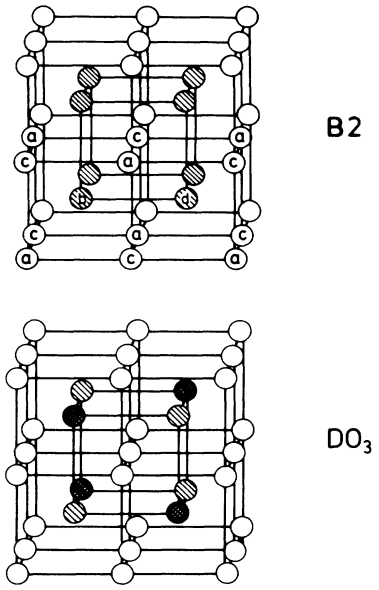

FIG. 1. Body-centered-cubic lattice showing the $B2$ structure (upper part) and DO_3 structure (lower part). Upper part shows assignment of four sublattices a,b,c,d. In the $A2$ structure, the average concentrations of A and B atoms are identical on all four sublattices while in the $B2$ structure the concentrations at the b and d sublattices are the same, but differ from the concentrations at the a and c sublattices, which again are the same (example: stoichiometric FeAl, with Fe on sublattices a and c; Al on sublattices b and d). In the DO_3 structure, the concentrations at the a and c sublattices still are the same, while the concentration at sublattice b differs from the concentration at sublattice d (example: stoichiometric Fe_3Al, with Al on sublattice b; all other sublattices taken by Fe).

II. THE MODEL, ITS ORDER PARAMETERS, SOME SYMMETRY CONSIDERATIONS, AND EXACT EXPANSIONS

Each lattice site i can exist in three states: It can be taken by an A atom with spin up (represented by an occupation variable $c_i = 1$, spin variable $\sigma_i = 1$), by an A atom with spin down ($c_i = 1$, $\sigma_i = -1$), or by a B atom ($c_i = 0$, no spin variable). The Hamiltonian chosen in this work then is

$$\mathcal{H} = \sum_{\langle i,j \rangle_{\mathrm{NN}}} \{c_i c_j (v_{\mathrm{NN}}^{AA} - J\sigma_i\sigma_j) + [(1-c_i)c_j + c_i(1-c_j)]v_{\mathrm{NN}}^{AB} + (1-c_i)(1-c_j)v_{\mathrm{NN}}^{BB}\}$$
$$+ \sum_{\langle i,j \rangle_{\mathrm{NNN}}} \{c_i c_j v_{\mathrm{NNN}}^{AA} + [(1-c_i)c_j + c_i(1-c_j)]v_{\mathrm{NNN}}^{AB} + (1-c_i)(1-c_j)v_{\mathrm{NNN}}^{BB}\} \ . \quad (1)$$

Thus, we allow for pairwise interactions only between nearest (NN) and next-nearest (NNN) neighbors; depending on the type of pair (AA, AB, or BB), these are denoted as v^{AA}, v^{AB}, and v^{BB}, respectively. The magnetic exchange interaction J is restricted to nearest neighbors only.

It is convenient to associate a spin variable $\sigma_i = 0$ to the B atoms. Then the magnetic part of the Hamiltonian, $-Jc_ic_j\sigma_i\sigma_j$ in Eq. (1), can also be written as $-J\sigma_i\sigma_j$. By the standard transformation to pseudospin variables $S_i = 2c_i - 1$ we obtain (μ being the chemical potential difference between A and B atoms)

$$\mathcal{H} - \mu \sum_i c_i = \mathcal{H}_0 + \mathcal{H}_I \ , \quad (2)$$

where $\mathcal{H}_0$ is a constant of no interest to us here and $\mathcal{H}_I$ is an Ising-type Hamiltonian

$$\mathcal{H}_I = W_{\mathrm{NN}} \sum_{\langle i,j \rangle_{\mathrm{NN}}} S_iS_j + W_{\mathrm{NNN}} \sum_{\langle i,j \rangle_{\mathrm{NNN}}} S_iS_j$$
$$- J \sum_{\langle i,j \rangle_{\mathrm{NN}}} \sigma_i\sigma_j - H \sum_i S_i \ . \quad (3)$$

In Eq. (3), the interaction parameters W_{NN}, W_{NNN}, and H are defined by

$$W_{\mathrm{NN}} = (v_{\mathrm{NN}}^{AA} + v_{\mathrm{NN}}^{BB} - 2v_{\mathrm{NN}}^{AB})/4 \ , \quad (4a)$$

$$W_{\mathrm{NNN}} = (v_{\mathrm{NNN}}^{AA} + v_{\mathrm{NNN}}^{BB} - 2v_{\mathrm{NNN}}^{AB})/4 \ , \quad (4b)$$

$$H = -2(v_{\mathrm{NN}}^{AA} - v_{\mathrm{NN}}^{BB}) - \tfrac{3}{2}(v_{\mathrm{NNN}}^{AA} - v_{\mathrm{NNN}}^{BB}) + \tfrac{1}{2}\mu \ . \quad (4c)$$

Note that in Eq. (3) the variables σ_i and S_i are not uncoupled from each other: $\sigma_i = 0$ if $S_i = -1$ while $\sigma_i = \pm 1$ if $S_i = +1$.

We now introduce sublattices a, b, c, d (Fig. 1) and

define sublattice pseudospin magnetizations m_μ ($\mu=a,b,c,d$) as

$$m_\mu \equiv \frac{1}{N}\sum_{i\in\mu} S_i, \quad m \equiv \sum_\mu m_\mu \ , \tag{5}$$

while the actual magnetization of the model is denoted as

$$M \equiv \frac{1}{N}\sum_i \sigma_i \ . \tag{6}$$

We now define order parameters ψ_1, ψ_2, ψ_3 as

$$\psi_1 \equiv m_a + m_c - m_b - m_d \tag{7}$$

and

$$\psi_2 \equiv m_a - m_c + m_b - m_d, \quad \psi_3 \equiv -m_a + m_c + m_b - m_d \ . \tag{8}$$

With the help of the order parameters $\langle M\rangle$, $\langle\psi_1\rangle$, $\langle\psi_2\rangle$, $\langle\psi_3\rangle$ all ordered phases occurring in the present model can be characterized: phases with $\langle M\rangle\neq 0$ are ferromagnetic, phases with $\langle M\rangle=0$ are paramagnetic. The phase with $\langle\psi_1\rangle=\langle\psi_2\rangle=\langle\psi_3\rangle=0$ has $\langle m_a\rangle=\langle m_b\rangle=\langle m_c\rangle=\langle m_d\rangle=\langle m\rangle/4$, i.e., there is no preferential occupation of any of the sublattices in Fig. 1: this is the $A2$ phase. In contrast, if $\langle m_a\rangle=\langle m_c\rangle\neq\langle m_b\rangle=\langle m_d\rangle$, we have $\langle\psi_1\rangle\neq 0$, while $\langle\psi_2\rangle=\langle\psi_3\rangle=0$. This phase is the $B2$ phase. Finally, the DO_3 phase is characterized by $\langle m_a\rangle=\langle m_c\rangle\neq\langle m_b\rangle\neq\langle m_d\rangle$ or $\langle m_b\rangle=\langle m_d\rangle\neq\langle m_a\rangle\neq\langle m_c\rangle$. In these cases we either have $\langle\psi_1\rangle\neq 0$, $\langle\psi_2\rangle=\langle\psi_3\rangle\neq 0$ or $\langle\psi_1\rangle\neq 0, \langle\psi_2\rangle=-\langle\psi_3\rangle\neq 0$. Landau symmetry rules[37] allow second-order transitions between the DO_3 phase and the $B2$ phase and between the $B2$ phase and the disordered $A2$ phase. In contrast, a direct transition from DO_3 to the $A2$ phase must be first order, if it occurs. This is seen considering the Landau expansion of the free energy F in terms of ψ_1, ψ_2, ψ_3 at given temperature T and concentration $\langle c\rangle=\langle\sum_i c_i\rangle/N$, for $M=0$,

$$F = F_0(T,\langle c\rangle) + r_1(T,\langle c\rangle)\psi_1^2 + r_2(T,\langle c\rangle)(\psi_2^2+\psi_3^2) + \cdots \ , \tag{9a}$$

where $F_0(T,\langle c\rangle)$ is the free energy when all order parameters are zero, and r_1, r_2 are suitable coefficients. This structure of the Landau expansion can be understood from the symmetry against relabeling of the sublattices: These transformations yield sign changes of the order parameters ψ_1, ψ_2, ψ_3 as well as an exchange of ψ_2 with ψ_3.[36] Now in Landau theory, a second-order transition from $A2$ to DO_3 would require that $r_1(T,\langle c\rangle)=r_2(T,\langle c\rangle)=0$, which can happen at most at isolated points in the phase diagram.[37] It is believed that this type of symmetry argument is valid beyond Landau theory. The same symmetry considerations as above yield as Landau expansions for the $A2$-$B2$ transition

$$F = F_0(T,\langle c\rangle) + r_1(T,\langle c\rangle)\psi_1^2 + u_1(T,\langle c\rangle)\psi_1^4 + \cdots \tag{9b}$$

and for the $B2$-DO_3 transition

$$F = F_0(T,\langle c\rangle) + r_2(T,\langle c\rangle)(\psi_2^2+\psi_3^2) + u_2(T,\langle c\rangle)(\psi_2^4+\psi_3^4) + u_3(T,\langle c\rangle)\psi_2^2\psi_3^2 + \cdots \ , \tag{9c}$$

where u_1, u_2, and u_3 are suitable coefficients.

Furthermore, the magnetic transition occurs either independently of the crystallographic order-disorder transitions as a second-order transition, or it must be of first order, if the magnetic order parameter vanishes together with crystallographic order. In addition, Eq. (9) suggests that there should also be a phase where $\langle\psi_1\rangle=0$ but $\langle\psi_2\rangle$ (or $\langle\psi_3\rangle$) is nonzero; this phase is realized if $\langle m_a\rangle=\langle m_b\rangle\neq\langle m_c\rangle=\langle m_d\rangle$ and gives rise to the $B32$ structure. For the choice of interactions of interest here, it is not realized, however. Finally, one can also provide a symmetry argument to show that a phase with all four sublattice pseudospin magnetizations $\langle m_\mu\rangle$ different from each other cannot occur.[36] Of course, more complicated structures than shown in Fig. 1 with more than four sublattices cannot *a priori* be excluded. However, an exact analysis of the ground states of the model Eq. (3), following the methods of Kanamori,[35] shows that at $T=0$ no other crystallographic structures than $A2$, $B2$, and DO_3 occur if we require

$$W_{\rm NN}>0, \quad W_{\rm NNN}>0, \quad 4W_{\rm NN}-6W_{\rm NNN}-J>0 \ . \tag{10}$$

The ground-state energies are then found as follows, normalized per lattice site

$$U_A/N = 4W_{\rm NN}+3W_{\rm NNN}-4J-H \quad (A2 \text{ structure, ferromagnetic}), \tag{11}$$
$$H > H_{c1} \equiv 8W_{\rm NN}+6W_{\rm NNN}-4J \ ,$$

$$U_{A_3B}/N = -2J-\tfrac{1}{2}H \quad (DO_3 \text{ structure, ferromagnetic}), \tag{12}$$
$$H_{c2} \equiv 8W_{\rm NN}-6W_{\rm NNN}-4J < H < H_{c1} \ ,$$

$$U_{AB}/N = -4W_{\rm NN}+3W_{\rm NNN} \quad (B2 \text{ structure, paramagnetic}), \tag{13}$$
$$H_{c3} \equiv -8W_{\rm NN}+6W_{\rm NNN} < H < H_{c2} \ ,$$

$$U_{AB_3}/N = \tfrac{1}{2}H \quad (DO_3 \text{ structure, paramagnetic}), \tag{14}$$
$$H_{c4} \equiv -8W_{\rm NN}-6W_{\rm NNN} < H < H_{c3} \ ,$$

and

$$U_B/N = 4W_{\rm NN}+3W_{\rm NNN}+H \quad (A2 \text{ structure, paramagnetic}), \quad H<H_{c4} \ . \tag{15}$$

In the following, we indicate briefly the lines of reason-

ing that yield[36] Eqs. (11)–(15). Since $J>0$, the minimum of energy always corresponds to a state where all A atoms have spin up (for structures such as AB or AB_3 each A atom is surrounded by nearest-neighbor B atoms and hence states with A atoms having spin down are energetically degenerate, but this degeneracy only matters for the ground-state entropy and not its energy). Hence it suffices to restrict attention to cases where a lattice site is either taken by an A atom with spin up or by a B atom. Then there are six possible states for the fundamental tetrahedron which has its corners at the four distinct sublattices (Fig. 2). Let us denote by p_i the probability that state i of a tetrahedron occurs in a considered state, with $\sum_{i=1}^{6} p_i = 1$. Then we may write

$$U/N = \sum_{i=1}^{6} E_i p_i \tag{16}$$

and obtain ground states by minimizing U with respect to the p_i; obeying the constraint $\sum_i p_i = 1$. The coefficients E_i in Eq. (16) are found as

$$\begin{aligned} E_1 &= 4W_{\mathrm{NN}} + 3W_{\mathrm{NNN}} - 4J - H \ , \\ E_2 &= 4W_{\mathrm{NN}} + 3W_{\mathrm{NNN}} + H \ , \\ E_3 &= -2J - \tfrac{1}{2}H \ , \\ E_4 &= \tfrac{1}{2}H \ , \\ E_5 &= -4W_{\mathrm{NN}} + 3W_{\mathrm{NNN}} \ , \\ E_6 &= -3W_{\mathrm{NNN}} - J \ . \end{aligned} \tag{17}$$

One can show that the ground states are just given by a filling of the lattice with a single tetrahedron configuration in each case; the configuration 6 in Fig. 2 would yield the $B32$ structure ($\langle m_a \rangle = \langle m_b \rangle \neq \langle m_c \rangle = \langle m_d \rangle$) which does not occur as a ground state if Eq. (10) holds, since then always $E_5 < E_6$. Conversely, if $4W_{\mathrm{NN}} - 6W_{\mathrm{NNN}} - J < 0$ (but still $W_{\mathrm{NN}} > 0$, $W_{\mathrm{NNN}} > 0$) the $B32$ structure would be stable instead of the $B2$ structure. The DO_3 phase is only stable if $W_{\mathrm{NNN}} > 0$.

Now it can be remarked that due to the magnetic degree of freedom the AB and AB_3 phases have nonzero ground-state entropies,

$$S_{AB}(T=0)/N = \frac{k_B}{2}\ln 2, \quad S_{AB_3}(T=0)/N = \frac{k_B}{4}\ln 2 \ , \tag{18}$$

while the ground-state entropy of all other phases is zero.

At this point, one can also comment on the order of the phase transitions at (and near) $T=0$. At H_{c1} we have a transition from phase $A2$ (pure A, ferromagnetic) to the ferromagnetic DO_3 structure (A_3B) which should be first order due to the symmetry argument quoted above. At H_{c2} we have a transition from the ferromagnetic DO_3 structure (A_3B) to the paramagnetic $B2$ structure (AB). This transition also must be of first order, since an analogous symmetry argument applies (ferromagnetic and crystallographic transitions coincide). The transition from the paramagnetic $B2$ structure (AB) to the paramagnetic DO_3 structure (AB_3) occurring at H_{c3} is not required to be first order by any symmetry argument. In addition, a consideration of the ground-state energies in the canonical ensemble of the alloy ($\langle c \rangle$ rather than μ being the independent variable) shows that there is also no lowering of the energy possible by a separation into coexisting pure phases.[36] The transition from the paramagnetic DO_3 structure (AB_3) to paramagnetic $A2$ (pure B) again has to be of first order.

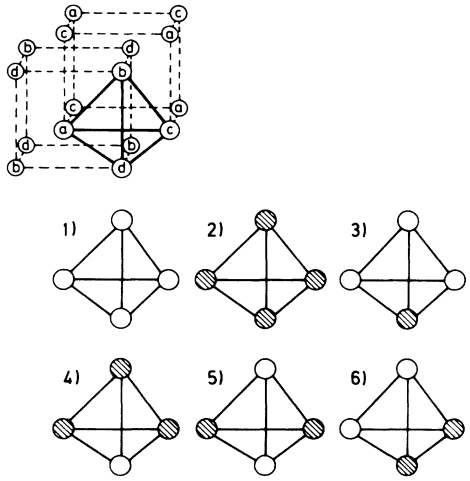

FIG. 2. Choice of basic tetrahedron in the structure (upper part) and six configurations of occupation by A atoms (open circles) or B atoms (shaded circles).

It is also useful to consider the leading terms of the low-temperature expansion in the various phases. We obtain[36]

$$F = U_0 - TS(T=0) - k_B T N \vartheta_\alpha \exp(-\varepsilon_\alpha / k_B T) \ , \tag{19}$$

where the ground-state energies U_0 of the various phases are listed in Eqs. (11)–(15), the ground-state entropies in Eq. (18), while the energies ε_α of the lowest excited states α and the degeneracy factors ϑ_α are listed below:

$$\varepsilon_1 = 16J, \quad \vartheta_1 = 1, \quad H > 8W_{\mathrm{NN}} + 6W_{\mathrm{NNN}} + 4J \ , \tag{20a}$$

$$\varepsilon_2 = -16W_{\mathrm{NN}} - 12W_{\mathrm{NNN}} + 8J + 2H, \quad \vartheta_2 = 1, \quad H_{c1} < H < 8W_{\mathrm{NN}} + 6W_{\mathrm{NNN}} + 4J \ , \tag{20b}$$

$$\varepsilon_3 = 16W_{\mathrm{NN}} + 12W_{\mathrm{NNN}} - 8J - 2H, \quad \vartheta_3 = \tfrac{1}{4}, \quad 8W_{\mathrm{NN}} + 6W_{\mathrm{NNN}} - 8J < H < H_{c1} \ , \tag{20c}$$

$$\varepsilon_4 = 8J, \quad \vartheta_4 = \tfrac{1}{2}, \quad 8W_{\mathrm{NN}} - 6W_{\mathrm{NNN}} < H < 8W_{\mathrm{NN}} + 6W_{\mathrm{NNN}} - 8J \ , \tag{20d}$$

$$\varepsilon_5 = -16W_{\mathrm{NN}} + 12W_{\mathrm{NNN}} + 8J + 2H, \quad \vartheta_5 = \tfrac{1}{4}, \quad H_{c2} < H < 8W_{\mathrm{NN}} - 6W_{\mathrm{NNN}} \ , \tag{20e}$$

$$\varepsilon_6 = 16W_{NN} - 12W_{NNN} - 8J - 2H, \quad \vartheta_6 = \tfrac{1}{256}, \quad -2J < H < H_{c2} , \tag{20f}$$

$$\varepsilon_7 = 16W_{NN} - 12W_{NNN} + 2H, \quad \vartheta_7 = \tfrac{1}{4}, \quad H_{c3} < H < -2J , \tag{20g}$$

$$\varepsilon_8 = -16W_{NN} + 12W_{NNN} - 2H, \quad \vartheta_8 = \tfrac{1}{2}, \quad -8W_{NN} < H < H_{c3} , \tag{20h}$$

$$\varepsilon_9 = 16W_{NN} + 12W_{NNN} + 2H, \quad \vartheta_9 = \tfrac{1}{8}, \quad H_{c4} < H < -8W_{NN} , \tag{20i}$$

$$\varepsilon_{10} = -16W_{NN} - 12W_{NNN} - 2H, \quad \vartheta_{10} = 2, \quad H < H_{c4} . \tag{20j}$$

It is seen that apart from the critical fields $H_{c1}, \ldots, H_{c4}$ where the ground-state structure changes, there are now further critical fields where the type of atomic excitation changes. Equations (20a) and (20b) both refer to the ground state where all sites are occupied by A atoms, having spin up, while the dominating excitation in the case of Eq. (20a) is a spin flip, and in the case of Eq. (20b) it is a change from A to B. In both cases $\vartheta = 1$, since every lattice site is available for this excitation. Similarly, the region $H_{c2} < H < H_{c1}$ where the ground state has sublattice d occupied with B and all other sublattices are occupied by A atoms having spin up, is split into three subregions where different excitations dominate: in the case of Eq. (20c), we consider a change from B to $A\uparrow$; here $\vartheta = \frac{1}{4}$ because only one sublattice out of four is available for this excitation. Note that the interval of Eq. (20d) only occurs for $3W_{NNN} > 2J$; here the excitation is a spin flip in sublattice a or sublattice c, and thus again the excitation energy is determined by magnetic exchange only, as in Eq. (20a)—but there are only half as many A neighbors. The excitation of Eq. (20e) is a change from A to B in sublattice b. Equations (20f) and (20g) refer to the AB phase as ground state (sublattices a and c taken by A atoms, sublattices b and d by B atoms, spin configuration arbitrary). Equation (20f) refers to a change $B \rightarrow A$; the quoted excitation energy applies only if in the resulting cluster of nine A atoms (the changed atom and its nearest neighbors) all spins are parallel—therefore we have such a low degeneracy factor. Equation (20g) describes a change from A to B. Here $\vartheta = \frac{1}{4}$ because $\frac{1}{2}$ of the sites are available for this excitation, and there are two ground states corresponding to only one excited state. Equations (20h) and (20i) refer to the AB_3 phase, with A atoms with arbitrary spin orientation on sublattice d. Now Eq. (20h) describes a change from B to A in sublattice b: although only $\frac{1}{4}$ of the sites are available, now two excited states correspond to one ground state and hence $\vartheta = \frac{1}{2}$. Equation (20i) refers to a change from A to B: $\frac{1}{4}$ of the sites are available and two ground states ($A\uparrow$, $A\downarrow$) correspond to one excited state, hence $\vartheta = \frac{1}{8}$. Finally, Eq. (20j) describes a change from B to $A\uparrow$ or $A\downarrow$ in a pure B phase. In the regime of a pure phase where different excitations dominate for different regimes of the field, one may simply add all terms referring to different excitations relative to the same phase, i.e.,

$$F = U_0 - TS(T=0) - k_B TN \sum_\alpha \vartheta_\alpha \exp(-\varepsilon_\alpha / k_B T) . \tag{21}$$

For example, for $H > H_{c1}$ Eq. (21) is a sum over two terms ($\alpha = 1,2$) and this expression then also is correct right at the critical field $H = 8W_{NN} + 6W_{NNN} + 4J$. Similarly, for $H_{c2} < H < H_{c1}$ Eq. (21) is a sum over three terms ($\alpha = 3,4,5$), etc. Equation (21) is justified from the general expression for the partition function Z,

$$Z = \Omega_0 \exp\left(-\frac{U_0}{k_B T}\right) + \sum_\alpha \Omega_\alpha \exp\left(-\frac{U_\alpha}{k_B T}\right) , \tag{22a}$$

where Ω_0 is the ground-state degeneracy and Ω_α are the degeneracies of the excited states having energies U_α; from Eq. (22a) we obtain, omitting higher-order terms,

$$\begin{aligned} F &= -k_B T \ln Z \\ &\cong U_0 - k_B T \ln \Omega_0 \\ &\quad - k_B T \sum_\alpha \frac{\Omega_\alpha}{\Omega_0} \exp\left(-\frac{U_\alpha - U_0}{k_B T}\right) + \cdots , \end{aligned} \tag{22b}$$

which is Eq. (21) if we define $\varepsilon_\alpha \equiv U_\alpha - U_0$, $\vartheta_\alpha \equiv \Omega_\alpha / (N\Omega_0)$, $S(T=0) \equiv k_B \ln \Omega_0$. The expansion is not applicable, however, in the vicinity of the critical fields $H_{c1}, \ldots, H_{c4}$: Eq. (20) shows that the energies ε_α of the lowest excited state vanish at these fields linearly with H. Hence the temperature region where the expansion is valid also decreases linearly with H, whereas at the critical field itself α just becomes a contribution to the (nontrivial) ground-state entropy.

As a final topic of this section, we also consider the high-temperature expansion of the free energy

$$\begin{aligned} F &= -k_B T \ln \left[\sum_{\{S_i, \sigma_i\}} \exp\left(-\frac{\mathcal{H}_I}{k_B T}\right) \right] \\ &= -k_B T \ln \left[3^N + \sum_{n=1}^{\infty} \frac{(-1)^n}{n!} \sum_{\{S_i, \sigma_i\}} \left(\frac{\mathcal{H}_I}{k_B T}\right)^n \right] . \end{aligned} \tag{23}$$

A somewhat tedious but straightforward calculation yields[36]

$$\begin{aligned} F/N = &-k_B T \ln 3 + \tfrac{4}{9} W_{NN} + \tfrac{1}{3} W_{NNN} - \tfrac{1}{3} H \\ &- \frac{4}{27 k_B T} \left[32 W_{NN}^2 + 20 W_{NNN}^2 + 6J^2 + 3H^2 \right. \\ &\quad + 32 W_{NN} W_{NNN} - 16 H W_{NN} \\ &\quad \left. - 12 W_{NNN} H \right] + O(T^{-2}) . \end{aligned} \tag{24}$$

This expansion explicitly illustrates the fact that unlike the standard Ising Hamiltonian the present model, Eq. (3), no longer possesses the symmetry $F(T,H)=F(T,-H)$. This lack of symmetry is due to the fact that the state $S_i=1$ is twofold degenerate ($\sigma_i=\pm 1$) while the state $S_i=-1$ is nondegenerate ($\sigma_i=0$). On the other hand, Eq. (1) is symmetric under the transformation $\{c_i\}\to\{1-c_i\}$ for $J=0$, which implies that for $J=0$ the phase diagram in the $(T,\langle c\rangle)$ plane is symmetric around the line $\langle c\rangle=\frac{1}{2}$. Another way to see this from Eq. (3) for $J=0$ is obtained[38] decomposing the partition function into the Boltzmann factor $\exp(-\mathcal{H}_I/k_BT)$ and the degeneracy factor $\Omega(\{S_i\})=2^{N_A}$, $N_A=(N+\sum_i S_i)/2$ being the total number of A atoms,

$$\begin{aligned} Z&=\sum_{\{S_i\}}\Omega(\{S_i\})\exp\left[-\mathcal{H}_I(\{S_i\})/k_BT\right] \\ &=2^{N/2}\sum_{\{S_i\}}\exp\left[\tfrac{1}{2}\ln 2\sum_i S_i\right]\exp[-\mathcal{H}_I(\{S_i\})/k_BT] \\ &=2^{N/2}\sum_{\{S_i\}}\exp[-\mathcal{H}_I'(\{S_i\})/k_BT]\ , \end{aligned} \tag{25}$$

where

$$\mathcal{H}_I'(\{S_i\})=W_{\rm NN}\sum_{\langle i,j\rangle_{\rm NN}}S_iS_j+W_{\rm NNN}\sum_{\langle i,j\rangle_{\rm NNN}}S_iS_j-H'\sum_i S_i\ ,$$

with

$$H'=H+\frac{k_BT}{2}\ln 2\ . \tag{26}$$

The Hamiltonian $\mathcal{H}_I'(\{S_i\})$ in Eq. (25) has the full Ising-model symmetry and hence we now have $F(T,H')=F(T,-H')$, with a redefined magnetic field H', Eq. (26).

III. CALCULATION OF THE PHASE DIAGRAM BY THE BRAGG-WILLIAMS MEAN-FIELD APPROXIMATION

We introduce the probability $p(\alpha,l)$ that on the sublattice α ($\alpha=a$, b, c, or d) one finds the state l ($l=1,2,3$), where $S=1$, $\sigma=1$ is represented by $l=1$, $S=1$, $\sigma=-1$ by $l=2$, and finally $S=-1$, $\sigma=0$ by $l=3$. Normalization of probabilities requires

$$\sum_{l=1}^{3}p(\alpha,l)=1\quad\text{for all }\alpha\ . \tag{27}$$

The entropy of a configuration is then simply given by

$$S=-k_BN\tfrac{1}{4}\textstyle\sum_{\alpha,l}p(\alpha,l)\ln p(\alpha,l)\ .$$

In the Bragg-Williams approximation, the energy term also is expressed in terms of the $p(\alpha,l)$. This is accomplished by factorizing the probability that a site on sublattice α is in state l and that a site on sublattice α' is in state l', the two sites being connected by a nearest-neighbor bond or a next-nearest-neighbor bond, respectively, into the product $p(\alpha,l)p(\alpha',l')$. Then the free energy is written

$$\begin{aligned} \frac{1}{N}F_{\rm BW}=&\sum_{l,l'}\{E_{\rm NN}(l,l')[p(a,l)p(b,l')+p(b,l)p(c,l')+p(c,l)p(d,l')+p(d,l)p(a,l')] \\ &+\tfrac{3}{2}E_{\rm NNN}(l,l')[p(a,l)p(c,l')+p(b,l)p(d,l')]\} \\ &-\frac{H}{4}\sum_{\alpha}[p(\alpha,1)+p(\alpha,2)-p(\alpha,3)]+k_BT\tfrac{1}{4}\sum_{\alpha,l}p(\alpha,l)\ln p(\alpha,l)\ , \end{aligned} \tag{28}$$

where the following abbreviations were introduced [note $E_{\rm NN}(l,l')=E_{\rm NN}(l',l)$, $E_{\rm NNN}(l,l')=E_{\rm NNN}(l',l)$]:

$$E_{\rm NN}(1,1)=E_{\rm NN}(2,2)=W_{\rm NN}-J\ , \tag{29a}$$

$$E_{\rm NN}(3,3)=W_{\rm NN}\ , \tag{29b}$$

$$E_{\rm NN}(1,2)=W_{\rm NN}+J\ , \tag{29c}$$

$$E_{\rm NN}(1,3)=E_{\rm NN}(2,3)=-W_{\rm NN}\ , \tag{29d}$$

$$E_{\rm NNN}(1,1)=E_{\rm NNN}(2,2)=E_{\rm NNN}(3,3)=E_{\rm NNN}(1,2)=W_{\rm NNN}\ , \tag{29e}$$

$$E_{\rm NNN}(1,3)=E_{\rm NNN}(2,3)=-W_{\rm NNN}\ . \tag{29f}$$

Now $F_{\rm BW}$ must be minimized with respect to the twelve variables $p(\alpha,l)$, subject to the four constraints written in Eq. (27) which are taken into account by the method of Lagrange multipliers. After some algebra this yields the following set of equations:[36]

$$\begin{aligned} p(\alpha,1)=\Bigg[2+x+\exp\Bigg[\frac{1}{k_BT}\{4[8W_{\rm NN}+(4W_{\rm NN}+J)y][p(b,1)+p(d,1)] \\ +24W_{\rm NNN}(2+x)p(c,1)-16W_{\rm NN}-12W_{\rm NNN}-2H\}\Bigg]\Bigg]^{-1}\ , \end{aligned} \tag{30a}$$

$$p(b,1)=\left[2+y+\exp\left[\frac{1}{k_BT}\{4[8W_{\mathrm{NN}}+(4W_{\mathrm{NN}}+J)x][p(a,1)+p(c,1)] +24W_{\mathrm{NNN}}(2+y)p(d,1)-16W_{\mathrm{NN}}-12W_{\mathrm{NNN}}-2H\}\right]\right]^{-1}, \tag{30b}$$

$$p(c,1)=\left[2+x+\left[\frac{1}{p(a,1)}-2-x\right]\exp\left[\frac{1}{k_BT}24W_{\mathrm{NNN}}(2+x)[p(a,1)-p(c,1)]\right]\right]^{-1}, \tag{30c}$$

$$p(d,1)=\left[2+y+\left[\frac{1}{p(b,1)}-2-y\right]\exp\left[\frac{1}{k_BT}24W_{\mathrm{NNN}}(2+y)[p(b,1)-p(d,1)]\right]\right]^{-1}, \tag{30d}$$

$$x=\exp\left[\frac{8J}{k_BT}y[p(b,1)+p(d,1)]\right]-1, \tag{30e}$$

$$y=\exp\left[\frac{8J}{k_BT}x[p(a,1)+p(c,1)]\right]-1. \tag{30f}$$

Note that there are only six instead of eight equations, due to two symmetry relations which follow from the minimization of F_{BW},

$$\frac{p(a,1)}{p(a,2)}=\frac{p(c,1)}{p(c,2)},\quad \frac{p(b,1)}{p(b,2)}=\frac{p(d,1)}{p(d,2)}. \tag{31}$$

The quantities x and y in Eq. (30) are auxiliary variables defined by

$$p(a,2)\equiv p(a,1)(1+x),\quad p(b,2)\equiv p(b,1)(1+y). \tag{32}$$

With the help of Eqs. (27), (31), and (32) all $p(\alpha,2)$ and $p(\alpha,3)$ can hence be expressed in terms of the $p(\alpha,1)$ and x and y. In the magnetically disordered phase, $x=y=0$.

We have written the result for the Bragg-Williams approximation in such detail since previous work on this model (or related models) claimed[31,32] that the probability of spin up and the probability of spin down are independent of the sublattice, which in addition to Eq. (31) would also imply

$$\frac{p(a,1)}{p(a,2)}=\frac{p(b,1)}{p(b,2)}\quad\text{or } x=y. \tag{33}$$

The explicit solution of Eqs. (30) in the ferromagnetic $B2$ and DO_3 phases shows, however, that Eq. (33) is not correct in general: Magnetic and crystallographic order are correlated to each other already on the level of the mean-field approximation. Explicitly, this is easily seen in the ferromagnetic $B2$ phase, where $p(a,1)=p(c,1)\neq p(b,1)=p(d,1)$, $x\neq 0$, $y\neq 0$. Assuming that $x=y$, Eqs. (30e) and (30f) are reduced to

$$x=\exp\left[\frac{16J}{k_BT}xp(b,1)\right]-1=\exp\left[\frac{16J}{k_BT}xp(a,1)\right]-1,$$

yielding $p(a,1)=p(b,1)$ in contradiction to the premises of a $B2$ phase.

In general, Eqs. (30) must be solved numerically. Defining a vector $\mathbf{p}\equiv(p(a,1),p(b,1),p(c,1),p(d,1),x,y)$, Eqs. (30) can be symbolically written as

$$\mathbf{p}=\Phi(\mathbf{p}), \tag{34}$$

with $\Phi(\mathbf{p})$ being defined as the right-hand side of Eqs. (30). The solution is obtained by looking for fixed points $\mathbf{p}^*$ of the iteration map

$$\mathbf{p}_{\nu+1}\equiv\tfrac{1}{2}[\mathbf{p}_\nu+\Phi(\mathbf{p}_\nu)],\quad \nu=1,2,\ldots,\infty. \tag{35}$$

The particular form of Eq. (35) is chosen since the iteration $\mathbf{p}_{\nu+1}=\Phi(\mathbf{p}_\nu)$ is badly converging at low temperatures.

It turns out that a solution of the full set of six equations (30) is only necessary in the ferromagnetic DO_3 phase, while in all other phases symmetry relations can be used to reduce the set of equations considerably. For example, in the paramagnetic $A2$ phase $x=y=0$, $p(a,1)=p(b,1)=p(c,1)=p(d,1)\equiv p$; i.e., Eqs. (30) reduce to a single equation for $p\,(=\langle c\rangle/2$ in this case),

$$p=\left[2+\exp\left[\frac{1}{k_BT}[(64W_{\mathrm{NN}}+48W_{\mathrm{NNN}})p-16W_{\mathrm{NN}}-12W_{\mathrm{NNN}}-2H]\right]\right]^{-1}. \tag{36}$$

In the ferromagnetic $A2$ phase, we now have $x=y\neq 0$ and two equations to be solved,

$$p=\left[2+x+\exp\left[\frac{1}{k_BT}\{8[8W_{\mathrm{NN}}+(4W_{\mathrm{NN}}+J)x]p +24W_{\mathrm{NNN}}(2+x)p-16W_{\mathrm{NN}}-12W_{\mathrm{NNN}}-2H\}\right]\right]^{-1}, \tag{37a}$$

$$x=\exp\left[\frac{1}{k_BT}16Jxp\right]-1. \tag{37b}$$

Linearizing the exponential function in Eq. (37b), we find the expected result for the Curie temperature $T_C(F)$ of the transition from paramagnetic to ferromagnetic $A2$,

$$\frac{k_B T_C(F)}{8J} = \langle c \rangle \ . \tag{38}$$

As expected, T_C decreases linearly with the concentration of the magnetic atoms.

Next we consider the paramagnetic $B2$ phase where $p(a,1)=p(c,1)=\frac{1}{4}(1+m+\psi_1)$, $p(b,1)=p(d,1)=\frac{1}{4}(1+m-\psi_1)$, $x=y=0$. After some algebra Eqs. (30) are reduced to[36]

$$(8W_{\rm NN}+6W_{\rm NNN})m + \frac{k_B T}{4}\ln\left[\frac{1}{4}\frac{1+m+\psi_1}{1-m-\psi_1}\frac{1+m-\psi_1}{1-m+\psi_1}\right]=H \ , \tag{39a}$$

$$(8W_{\rm NN}-6W_{\rm NNN})\psi_1 + \frac{k_B T}{4}\ln\left[\frac{1+m-\psi_1}{1+m+\psi_1}\frac{1-m-\psi_1}{1-m+\psi_1}\right]=0 \ . \tag{39b}$$

Expanding Eq. (39b) for small ψ_1 yields the critical temperature $T_C(AB)$ of the $A2$-$B2$ transition

$$k_B T_C(AB)=(8W_{\rm NN}-6W_{\rm NNN})(1-\langle m \rangle^2) = (32W_{\rm NN}-24W_{\rm NNN})\langle c \rangle(1-\langle c \rangle) \ , \tag{40}$$

which has the familiar parabolic shape in the $(T,\langle c \rangle)$ plane. Of course, Eq. (40) applies only where $T_C(AB)>T_C(F)$ and Eq. (38) applies only where $T_C(F)>T_C(AB)$, as we have always considered transitions to a fully disordered $A2$ phase. In addition, this calculation does not show that the transitions from the paramagnetic $A2$ phase to the ferromagnetic $A2$ phase or the paramagnetic $B2$ phase are actually second-order transitions; rather we have obtained $T_C(F)$ and $T_C(AB)$ as stability limits of the respective ordered phases. The second-order nature of these transitions is shown, however, by considering the Hessian matrix H_{mn} of second derivatives,

$$H_{mn}=\left[\frac{\partial^2 F/N}{\partial p_m \partial p_n}\right]_{p^*} \ , \tag{41}$$

in the disordered phase and showing that all eigenvalues are positive for $T>\max[T_C(F),T_C(AB)]$, while one eigenvalue changes sign at $T_C(F)$ [and another one changes sign at $T_C(AB)$]. The change of sign of these eigenvalues of the Hessian matrix simply reflects the Curie-Weiss laws for the ferromagnetic susceptibility and the staggered "susceptibility" conjugate to the order parameter of the $B2$ phase: In the paramagnetic $A2$ phase the Hessian matrix after diagonalization becomes[36]

$$H_{mn}^{\rm diag}=\chi_n^{-1}\delta_{mn}, \quad m,n=1,\ldots,6 \tag{42a}$$

with

$$\chi_4^{-1}\equiv\frac{\partial^2 F/N}{\partial m^2}=\frac{k_B T}{1-\langle m \rangle^2}+8W_{\rm NN}+6W_{\rm NNN} \ , \tag{42b}$$

$$\chi_1^{-1}\equiv\frac{\partial^2 F/N}{\partial \psi_1^2}=\frac{k_B T}{1-\langle m \rangle^2}-8W_{\rm NN}+6W_{\rm NNN} \ , \tag{42c}$$

$$\chi_2^{-1}\equiv\frac{\partial^2 F/N}{\partial \psi_2^2}=\chi_3^{-1}\equiv\frac{\partial^2 F/N}{\partial \psi_3^2}=\frac{k_B T}{1-\langle m \rangle^2}-6W_{\rm NNN} \ , \tag{42d}$$

$$\chi_5^{-1}\equiv\frac{\partial^2 F/N}{\partial M^2}=\frac{2k_B T}{1+\langle m \rangle}-8J \ , \tag{42e}$$

$$\chi_6^{-1}\equiv\frac{\partial^2 F/N}{\partial \tilde{M}^2}=\frac{2k_B T}{1+\langle m \rangle}+8J \ . \tag{42f}$$

Here χ_1,χ_2,χ_3 are just the response functions of F with respect to the order parameters ψ_1,ψ_2,ψ_3 [Eqs. (7) and (8)], χ_4 is the response function $\partial m/\partial H$ describing the change of concentration $\langle c \rangle$ with chemical potential changes, χ_5 is the ferromagnetic susceptibility [cf. Eq. (6)], and χ_6 is the antiferromagnetic (staggered) susceptibility. The quantity $\tilde{M}$, the staggered magnetization, is obtained in terms of the $p(\alpha,1)$, x, and y as

$$\tilde{M}=-\tfrac{1}{4}\{x[p(a,1)+p(c,1)]-y[p(b,1)+p(d,1)]\} \ , \tag{43a}$$

while the magnetization M is given by

$$M=-\tfrac{1}{4}\{x[p(a,1)+p(c,1)]+y[p(b,1)+p(d,1)]\} \ , \tag{43b}$$

and m, ψ_1, ψ_2, ψ_3 are expressed in terms of the $p(\alpha,1)$, x, and y as

$$m=[p(a,1)+p(c,1)](1+x/2) + [p(b,1)+p(d,1)](1+y/2)-1 \ , \tag{43c}$$

$$\psi_1=[p(a,1)+p(c,1)](1+x/2) - [p(b,1)+p(d,1)](1+y/2) \ , \tag{43d}$$

$$\psi_2=[p(a,1)-p(c,1)](1+x/2) + [p(b,1)-p(d,1)](1+y/2) \ , \tag{43e}$$

$$\psi_3=-[p(a,1)-p(c,1)](1+x/2) + [p(b,1)-p(d,1)](1+y/2) \ . \tag{43f}$$

Equations (43) are valid in all phases while Eq. (42) holds in the paramagnetic $A2$ phase only. The crystallographic ordering in the $B2$ or DO_3 phase has the consequence that the magnetization is no longer the same at all sublattices and then the magnetization M always is accompanied by a staggered magnetization $\tilde{M}$, Eq. (43a). This order parameter occurs only in the region of joint magnetic and crystallographic ordering, i.e., for temperatures below the multicritical point T_m, which occurs for $4W_{\rm NN}-3W_{\rm NNN}>J$ at

$$\langle c \rangle = 1-\frac{J}{4W_{\rm NN}-3W_{\rm NNN}}, \quad k_B T_m = 8J-\frac{8J^2}{4W_{\rm NN}-3W_{\rm NNN}} \ . \tag{44}$$

It is also of interest to study in more detail the ferromagnetic $B2$ phase where Eqs. (30) (written in terms of m, ψ_1, M, $\tilde{M}$) reduce to

$$(8W_{\mathrm{NN}}+6W_{\mathrm{NNN}})m-4JM+\frac{k_BT}{4}\ln\left[\frac{1}{4}\frac{(1+m+2M)^2-(\psi_1+2\tilde{M})^2}{(1-m)^2-\psi_1^2}\right]=H\ , \tag{45a}$$

$$(8W_{\mathrm{NN}}-6W_{\mathrm{NNN}})\psi_1-4J\tilde{M}-\frac{k_BT}{4}\ln\left[\frac{1+m+2M+\psi_1+2\tilde{M}}{1+m+2M-\psi_1-2\tilde{M}}\frac{1-m+\psi_1}{1-m-\psi_1}\right]=0\ , \tag{45b}$$

$$8JM+\frac{k_BT}{4}\ln\left[\frac{(1+m-2M)^2-(\psi_1-2\tilde{M})^2}{(1+m+2M)^2-(\psi_1+2\tilde{M})^2}\right]=0\ , \tag{45c}$$

$$8J\tilde{M}-\frac{k_BT}{4}\ln\left[\frac{(1+m-2\tilde{M})^2-(\psi_1-2M)^2}{(1+m+2\tilde{M})^2-(\psi_1+2M)^2}\right]=0\ . \tag{45d}$$

Expanding (45c) and (45d) for small M and $\tilde{M}$, one obtains for the magnetic transition

$$k_BT_C(F)=8J\left[\left[\frac{1+\langle m\rangle}{2}\right]^2-\frac{\langle\psi_1\rangle^2}{4}\right]^{1/2}=8J(\langle c\rangle^2-\langle\psi_1\rangle^2/4)^{1/2}\ . \tag{46a}$$

Similarly, expanding (45b) and (45d) for small ψ_1 and $\tilde{M}$ yields for the AB transition

$$\begin{aligned}k_BT_C(AB)=&(4W_{\mathrm{NN}}-3W_{\mathrm{NNN}})(1-\langle m\rangle^2)-2J(1+\langle m\rangle-2\langle M\rangle^2)\\&+\{[(4W_{\mathrm{NN}}-3W_{\mathrm{NNN}})(1-\langle m\rangle^2)]^2+[2J(1+\langle m\rangle-2\langle M\rangle^2)]^2\\&+4J(4W_{\mathrm{NN}}-3W_{\mathrm{NNN}})(1-\langle M\rangle)[(1+\langle m\rangle)^2-2\langle M\rangle^2(3-\langle m\rangle)]\}^{1/2}\ .\end{aligned} \tag{46b}$$

Near the multicritical point in the ordered phases, we have

$$\langle\psi_1\rangle^2\propto T_C(AB)-T,\quad \langle M\rangle^2\propto T_C(F)-T\ ,$$

and therefore both lines have a kink at this point. Carrying the expansion of (45c) and (45d) to third order in M and $\tilde{M}$, we obtain

$$\langle M\rangle\approx\sqrt{3\varepsilon}\left[\langle c\rangle^2-\frac{\langle\psi_1\rangle^2}{4}\right]^{1/2}\times\frac{1}{2}\left[\left[1+\frac{\langle\psi_1\rangle}{2\langle c\rangle}\right]^{1/2}+\left[1-\frac{\langle\psi_1\rangle}{2\langle c\rangle}\right]^{1/2}\right] \tag{47a}$$

and

$$\langle\tilde{M}\rangle\approx\sqrt{3\varepsilon}\left[\langle c\rangle^2-\frac{\langle\psi_1\rangle^2}{4}\right]^{1/2}\times\frac{1}{2}\left[\left[1+\frac{\langle\psi_1\rangle}{2\langle c\rangle}\right]^{1/2}-\left[1-\frac{\langle\psi_1\rangle}{2\langle c\rangle}\right]^{1/2}\right] \tag{47b}$$

with

$$\varepsilon=1-\frac{T}{T_C(F)}\ . \tag{47c}$$

These results analytically demonstrate the existence of a staggered magnetization induced by the existence of the order parameter ψ_1, as anticipated above.

The phase boundaries of the paramagnetic and ferromagnetic DO_3 phases have been found numerically, by the iteration method outlined in Eq. (35) starting out in ordered phases and looking for the temperatures where the order parameters ψ_2 and ψ_3 vanish; in addition, the Hessian matrix H_{mn} [Eq. (41)] has been diagonalized by computer programs to show via the vanishing of the eigenvalues corresponding to χ_2^{-1} and χ_3^{-1} in the ordered phases that the phase transitions are actually second order. It turns out, however, that at low temperatures parts of the $DO_3\rightarrow B2$ phase transitions actually are first order. There it is necessary to start the iteration in both the DO_3 and $B2$ phases, and to use the respective solutions $\mathbf{p}^*(B2)$ and $\mathbf{p}^*(DO_3)$ to compute the free energy F_{BW}, Eq. (28), and locate the first-order phase transitions by the intersection of the two free-energy branches. For the case actually studied numerically,

$$\frac{W_{\mathrm{NNN}}}{W_{\mathrm{NN}}}=0.5,\quad \frac{J}{W_{\mathrm{NN}}}=0.7\ , \tag{48}$$

a direct first-order DO_3-$A2$ transition did not occur on the paramagnetic (B-rich) side of the phase diagram, whereas it did occur on the ferromagnetic side. We defer a discussion of the numerically obtained phase diagram to the next section where it will be compared to the cluster-variation result.

IV. CALCULATION OF THE PHASE DIAGRAM BY THE CLUSTER-VARIATION METHOD IN THE TETRAHEDRON APPROXIMATION

In this section we briefly describe our application of the cluster-variation method[26] to the present problem. The general spirit of the approach is very similar to previous work on other alloy-ordering problems with this method;[7–9,29,39–43] we hence only summarize the main

points. Very similar considerations in more detail for the fcc case can be found, e.g., in Kikuchi, Ref. 7. The analysis is based on the same tetrahedron on which the ground-state analysis was based (Fig. 2), and considers the probability $p_{abcd}(l,l',l'',l''')$ that the tetrahedron atom belonging to sublattice a is in state l, the atom belonging to sublattice b is in state l', etc. (tetrahedron variables; the labeling of states is the same as the preceding section). As is well known,[7,9,19,39–43] one must consider all subclusters of the chosen basic cluster (triangles, NN and NNN pairs and points in our case) and the analogously defined subcluster variables such as $p_{abc}(l,l',l'')$, $p_{bcd}(l,l',l'')$, $p_{ab}(l,l')$, $p_{ac}(l,l')$, $p_a(l)$, etc., which are related to the tetrahedron variables by simple recursion relations. Now the free energy $F=U-TS$ is expressed in terms of these probabilities to yield the free energy F_{CV} in the cluster variation (CV) approximation as $F_{\mathrm{CV}}=U_{\mathrm{CV}}-TS_{\mathrm{CV}}$, where

$$\frac{1}{N}U(\{P_{abcd}\})\sum_{l,l',l'',l'''}E(l,l',l'',l''')\times p_{abcd}(l,l',l'',l''') \tag{49}$$

and $E(l,l',l'',l''')$ is written in terms of spin variables $S(l)$ and $\sigma(l)$ [$S(1)=S(2)=+1$, $S(3)=-1$, $\sigma(1)=+1$, $\sigma(2)=-1$, $\sigma(3)=0$] as

$$E(l,l',l'',l''')=W_{\mathrm{NN}}[S(l)S(l')+S(l')S(l'')+S(l'')S(l''')+S(l''')S(l)]+\tfrac{3}{2}W_{\mathrm{NNN}}[S(l)S(l'')+S(l')S(l''')]$$
$$-J[\sigma(l)\sigma(l')+\sigma(l')\sigma(l'')+\sigma(l'')\sigma(l''')+\sigma(l''')\sigma(l)]-H[S(l)+S(l')+S(l'')+S(l''')]/4\ . \tag{50}$$

Since we only have short-range interactions fitting into the tetrahedron, $U_{\mathrm{CV}}=U$ is an exact expression following directly from the Hamiltonian, Eq. (3), using the fact that each nearest-neighbor bond is shared by six tetrahedra, each next-nearest neighbor bond is shared by four tetrahedra, each corner by 24 tetrahedra and that there are $6N$ tetrahedra in a bcc lattice with N sites for $N\to\infty$. Hence factors $6\times\frac{1}{6}=1$ result for W_{NN} and J, but $6\times\frac{1}{4}=\frac{3}{2}$ for W_{NNN} and $6\times\frac{1}{24}=\frac{1}{4}$ for H.

The analogous expression S_{CV} for the entropy is approximate only (it would become exact in the limit of infinite cluster size[41]). A straightforward application of the standard procedures for deriving such expressions (see, e.g., Refs. 39 and 40) yields,[36,43] using the notation $\mathcal{L}(x)\equiv x\ln x$,

$$\frac{1}{k_BN}S_{\mathrm{CV}}=\tfrac{1}{4}\sum_l[\mathcal{L}(p_a(l))+\mathcal{L}(p_b(l))+\mathcal{L}(p_c(l))+\mathcal{L}(p_d(l))]$$
$$-\sum_{l,l'}[\mathcal{L}(p_{ab}(l,l'))+\mathcal{L}(p_{bc}(l,l'))+\mathcal{L}(p_{cd}(l,l'))+\mathcal{L}(p_{da}(l,l'))]-\tfrac{3}{2}\sum_{l,l'}[\mathcal{L}(p_{ac}(l,l'))+\mathcal{L}(p_{bd}(l,l'))]$$
$$+3\sum_{l,l',l''}[\mathcal{L}(p_{abc}(l,l',l''))+\mathcal{L}(p_{bcd}(l,l',l''))+\mathcal{L}(p_{cda}(l,l',l''))+\mathcal{L}(p_{dab}(l,l',l''))]$$
$$-6\sum_{l,l',l'',l'''}\mathcal{L}(p_{abcd}(l,l',l'',l'''))\ . \tag{51}$$

Minimizing F_{CV} with respect to the tetrahedron variables, one must take into account the recursion relations for the subcluster variables as well as the normalization condition for the tetrahedron probabilities, the latter being done by a Lagrange multiplier Λ. One then obtains (cf. also Ref. 43)

$$p_{abcd}(l,l',l'',l''')=\exp\left[\frac{\Lambda}{6k_BT}\right]P_{abcd}(l,l',l'',l''')\ , \tag{52}$$

where the unnormalized probabilities P_{abcd} are given by

$$P_{abcd}(l,l',l'',l''')\equiv\exp\left[-\frac{E(l,l',l'',l''')}{6k_BT}\right]\frac{[p_a(l)p_b(l')p_c(l'')p_d(l''')]^{1/24}}{[p_{ab}(l,l')p_{bc}(l',l'')p_{cd}(l'',l''')p_{da}(l''',l)]^{1/6}}$$
$$\times\frac{[p_{abc}(l,l',l'')p_{bcd}(l',l'',l''')p_{cda}(l'',l''',l)p_{dab}(l''',l,l')]^{1/2}}{[p_{ac}(l,l'')p_{bd}(l',l''')]^{1/4}}\ . \tag{53}$$

Defining a "partition function" Z as

$$Z\equiv\sum_{l,l',l'',l'''}P_{abcd}(l,l',l'',l''')\ , \tag{54}$$

the normalization of the tetrahedron variables implies

$$\Lambda=-6k_BT\ln Z\ . \tag{55}$$

From the minimization procedure it follows that in equilibrium

$$F_{\mathrm{CV}}=\Lambda N\ . \tag{56}$$

We did not attempt to reduce the number of variables in the various phases by the use of symmetry relations, as has been done, e.g., in Ref. 19, but rather used Kikuchi's[7] simple "natural iteration" algorithm with the full set of tetrahedron variables in all phases:

(i) Choice of a starting distribution $\{p_{abcd}(l,l',l'',l''')\}$.

(ii) Calculation of the subcluster probabilities.

(iii) Calculation of $\{P_{abcd}(l,l',l'',l''')\}$ from Eq. (53).

(iv) Calculation of Λ from Eqs. (54) and (55).

(v) Calculation of the new tetrahedron variables from Eq. (52).

At high temperatures off the phase boundaries, a few hundred iterations were sufficient to obtain four significant decimal places in F_{CV}. Close to second-order boundaries in the ordered phases, longer iterations are necessary: Sometimes the convergence was still unsatisfactory after 8000 or 10 000 iterations (2000 iterations take about 5 min at a Honeywell-Bull PDS8 computer). Second-order phase boundaries are located precisely by computing the Hessian matrix

$$H_{nn'} \equiv \frac{\partial^2 F/N}{\partial p_{abcd}(l,l',l'',l''')\partial p_{abcd}(m,m',m'',m''')} , \quad (57)$$

and locating the point where the smallest eigenvalues vanishes. This involves the numerical diagonalization of 80×80 matrices [the index n in Eq. (57) labels the 80 independent variables $\{p_{abcd}(l,l',l'',l''')\}$, one variable being eliminated by the normalization condition].

This "natural iteration method" conserves any symmetries present in the initial values $\{p_{abcd}(l,l',l'',l''')\}$, if these are also symmetries of the Hamiltonian. Thus the "broken symmetry" appropriate for each ordered phase has to be put in "by hand" choosing initial values exhibiting the proper symmetry breaking. We have done this by first obtaining equilibrium data for $\{p_{abcd}(l,l',l'',l''')\}$ in the disordered $A2$ phase, for which the algorithm converges best, cooling down the temperature in small enough steps from initially high temperatures, and locating the zero of the smallest eigenvalue of the Hessian matrix. In the ordered phase, we first apply a symmetry-breaking field so that the iteration yields some $\{p_{abcd}(l,l',l'',l''')\}$ with the desired symmetry breaking, and then take these values as initial values for an iteration which switched-off fields and so obtain "spontaneous ordering." Such states in turn can be used as an initial configuration for a neighboring temperature (or field) in the phase diagram. We found it necessary to apply "slow cooling" procedures (i.e., starting each iteration from an equilibrium configuration only a small distance in reduced temperature $k_B\Delta T/W_{NN} \ll 1$ or reduced field $\Delta H/W_{NN} \ll 1$ away), because otherwise some of the $p_{abcd}(l,l',l'',l''')$ appearing during the iteration [see cases (i)–(v) given above] would be so small (due to the factor $\exp[-E(l,l,l'',l''')/6k_BT]$) that the program takes them equal to zero, which is not an allowed value. Even with this time-consuming "slow-cooling" technique, we have not been able to treat temperatures lower than about $k_BT/W_{NN} \approx 1$, for the model Eq. (48).

Figures 3–5 now summarize our numerical results for this model and show that there is a significant discrepancy between the mean-field phase diagram and the cluster-variation phase diagram, both in qualitative and in quantitative respects. (i) The mean-field approximation overestimates the regime of stability of each ordered phase typically by a factor as large as 1.5. (ii) The mean-field approximation predicts that the system leaves the disordered phase for strongly negative H/W_{NN} by a second-order transition to the paramagnetic $B2$ phase, and only at lower temperature can a first-order $B2$-DO_3 transition occur. In contrast, the cluster-variation method predicts direct first-order $A2$-DO_3 transitions, without an intervening $B2$ phase, for a broad range of fields. (iii) The mean-field approximation predicts a reentrant phase boundary at negative H/W_{NN} for both the $B2$ phase and the DO_3 phase. In the regime

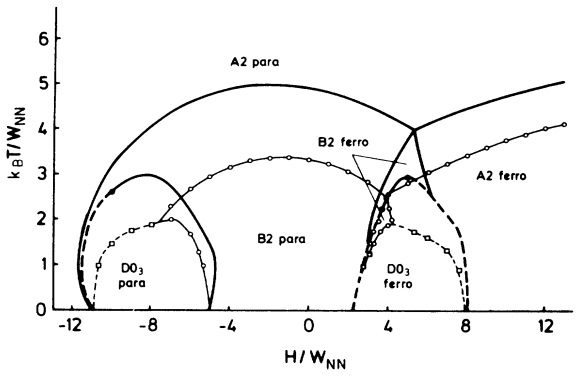

FIG. 3. Comparison of the phase diagram predicted by the Bragg-Williams mean-field approximation (thick lines) to the phase diagram predicted by the cluster-variation method in the tetrahedron approximation (thin lines), in the grand-canonical ensemble, for $W_{NNN}/W_{NN}=0.5$, $J/W_{NN}=0.7$. Solid dots denote tricritical points as found in the mean-field approximation. Second order transitions are denoted by solid curves; first-order transitions by dashed curves. The cluster-variation calculation has been carried out for particular points only, as indicated by circles (in the case of second-order transitions) or squares (in the case of first-order transitions), respectively. Nature of the various phases is indicated in the figure.

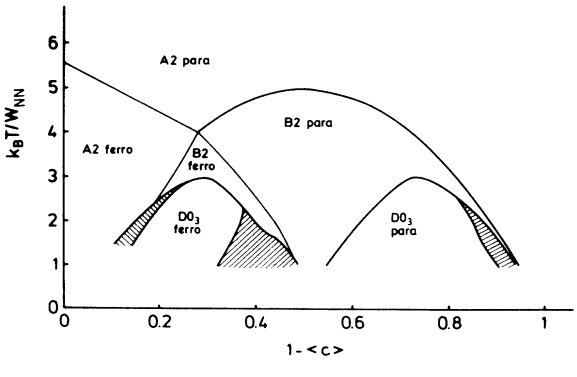

FIG. 4. Phase diagram of the model with $W_{NNN}/W_{NN}=0.5$ and $J/W_{NN}=0.7$ in the canonic ensemble as predicted by the Bragg-Williams mean-field approximation. Nature of the various pure phases is indicated in the figure; the shaded regions denote two-phase coexistence regions between the two adjoining pure phases.

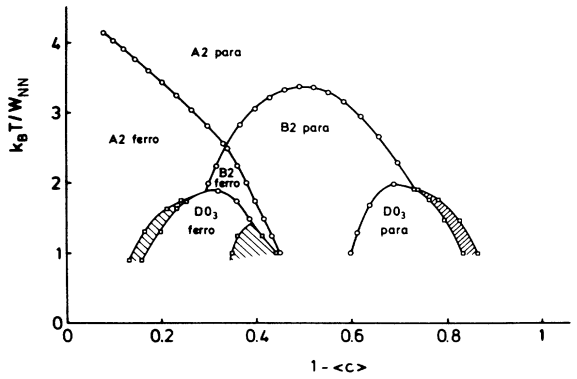

FIG. 5. Same as Fig. 4 but according to the cluster-variation method in tetrahedron approximation.

$-5<H/W_{\mathrm{NN}}\lesssim -4.6$ there is also a double transition $B2$-DO_3-$B2$ due to reentrant shape of the phase boundary near the critical field H_{c3}. Neither of these features of the phase diagram are confirmed by the cluster-variation calculation. These discrepancies also are pronounced in the canonic ensemble, as seen by a comparison between Figs. 4 and 5. It is seen that also the phase boundaries of the crystallographically ordered phases ($B2$, DO_3) on the left- and right-hand halves of the phase diagram are rather distinct from each other. This lack of symmetry around $\langle c\rangle=0.5$ reflects the interplay between crystallographic and magnetic order.

V. CALCULATION OF THE PHASE DIAGRAM BY THE MONTE CARLO METHOD

Unlike the methods described in Secs. III and IV, the application of the Monte Carlo method to the present problem is straightforward in principle—though tedious in practice because of the large amount of computing time needed. But the general approach to study phase transitions by Monte Carlo methods, as described elsewhere,[3,11,12,34,44] applies to the present problem too, and need not be repeated here. Hence we only emphasize that all Monte Carlo runs were performed for lattices of size $N=2L^3$, where $L=6$, 12, or 20, choosing periodic boundary conditions and a single-site algorithm. The transition probability was chosen as (where x_i denotes the initial and x_f the final state of the considered site: there are three choices both for the initial and the final state)

$$W(x_i\to x_f)=\begin{cases}\frac{1}{2} & \text{if } f\neq i,\ \mathcal{H}(x_f)\le\mathcal{H}(x_i)\ ,\\ \frac{1}{2}\exp\{-[\mathcal{H}(x_f)-\mathcal{H}(x_i)]/k_BT\} & \text{if } f\neq i,\ \mathcal{H}(x_f)>\mathcal{H}(x_i)\ ,\\ 1-\sum\limits_{f(\neq i)} W(x_i\to x_f) & \text{if } f=i\ .\end{cases} \tag{58}$$

It is convenient to realize the transitions $x_i\to x_f$ by dividing the interval from zero to unity in three parts I_1, I_2, I_3 with the lengths $W(x_i\to x_1)$, $W(x_i\to x_2)$, $W(x_i\to x_3)$. Then a random number uniformly distributed between zero and unity is drawn. If it falls in the interval I_k, we perform the move $x_i\to x_k$.

The Monte Carlo simulation is carried out in the grand canonical ensemble. Since in a finite system there is no broken symmetry in a strict sense (i.e., in a course of a Monte Carlo simulation the order parameters may spontaneously change their sign, except if sufficiently strong symmetry-breaking fields are applied), we record the following positive definite order parameters:

$$\langle\,|M|\,\rangle,\quad \langle\,|\psi_1|\,\rangle,\quad \langle(\psi_2^2+\psi_3^2)^{1/2}\rangle\ . \tag{59}$$

Here the order parameter of the DO_3 phase was symmetrized as is appropriate for an ordering with a two-component parameter. The specific heat (and the susceptibilities) were computed from the fluctuation relations

$$\frac{C}{k_B}=\frac{1}{N(k_BT)^2}(\langle\mathcal{H}^2\rangle-\langle\mathcal{H}\rangle^2)\ , \tag{60}$$

$$\chi_F=\frac{N}{k_BT}(\langle M^2\rangle-\langle\,|M|\,\rangle^2)\ , \tag{61}$$

$$\chi_1=\frac{N}{k_BT}(\langle\psi_1^2\rangle-\langle\,|\psi_1|\,\rangle^2)\ , \tag{62}$$

$$\chi_{DO_3}=\frac{N}{k_BT}[\langle(\psi_2^2+\psi_3^2)\rangle-\langle(\psi_2^2+\psi_3^2)^{1/2}\rangle^2]\ . \tag{63}$$

For locating second-order transitions, it is convenient to consider the normalized fourth-order cumulant of the order-parameter distribution[34,44]

$$U_F=1-\frac{\langle M^4\rangle}{3\langle M^2\rangle^2}\ , \tag{64}$$

$$U_1=1-\frac{\langle\psi_1^4\rangle}{3\langle\psi_1^2\rangle^2}\ , \tag{65}$$

$$U_{DO_3}=1-\frac{\langle\psi_2^4\rangle+\langle\psi_3^4\rangle}{3(\langle\psi_2^2\rangle^2+\langle\psi_3^2\rangle^2)}\ . \tag{66}$$

From the pseudospin magnetization $\langle m\rangle$ recorded as function of H we can make the standard translation from the grand canonical to the canonical ensemble of the alloy.[3,11] Second-order transitions then are located from peaks of the appropriate susceptibility [Fig. 6(a) shows an example] and/or from the intersection of cumulants [Eqs. (64)–(66)] recorded for different linear dimensions L [Fig. 6(b)]. Due to the smallness of the

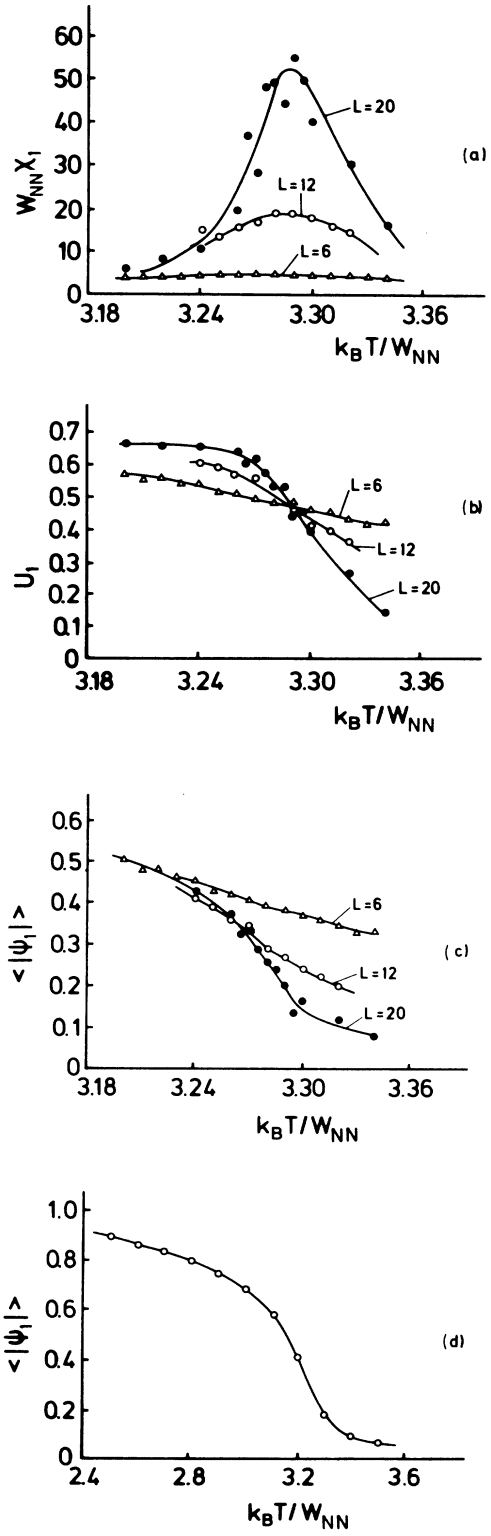

FIG. 6. (a) Susceptibility χ_1, (b) cumulant U_1, and (c) order parameter $\langle|\psi_1|\rangle$ plotted vs reduced temperature for $H/W_{NN}=-1$, using 20000 MCS/site and three different linear dimensions as indicated in the figure. (d) shows $\langle|\psi_1|\rangle$ plotted vs temperature for $H=0$, using 600 MCS/site and $L=12$. Curves are only guides to the eye.

simulated system, the variation of the order parameters with temperature in the transition region is rather smooth [Fig. 6(c)], and hence the cumulant intersection method must be used if one wishes to locate the transition temperature with a relative accuracy of 0.5% or better. This method, however, requires rather long runs [typically 20000 Monte Carlo steps (MCS) per site have to be used with additional 5000 equilibration steps at the beginning of the run being omitted[45]]. If one is satisfied with a description of a coarser temperature scale, locating a transition temperature with an accuracy of about 3% only, a short run (600 steps used, 200 steps omitted) with a medium size ($L=12$) is sufficient to record the order-parameter variation, the transition being located from the inflection point of such a curve [Fig. 6(d)]. The points with the large error bars in our phase diagrams below (Figs. 12 and 13) have been recorded with this rough method only, for the sake of an economic use of computer time.[46] However, for resolving cases where two different phase boundaries occur close together, as happens for the ferromagnetic $B2$ phase, the cumulant intersection method proves to be very valuable: Fig. 7 shows clearly that the decay of ferromagnetism occurs at a smaller value of H [Fig. 7(a)] than the decay of $B2$ or-

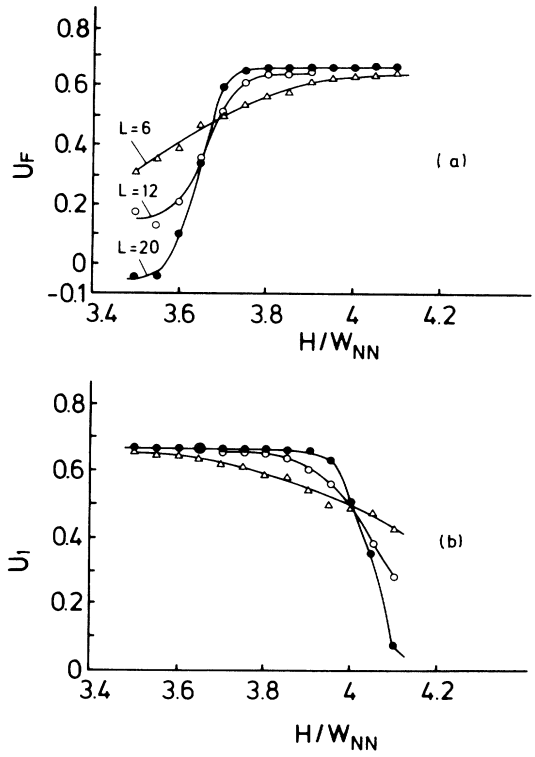

FIG. 7. Cumulant intersection plot for (a) the ferromagnetic order and (b) the $B2$ order for $k_BT/W_{NN}=2.1$, varying the field H/W_{NN}. Data for $L=6$ and 12 are based on 20000 MCS, while only 15000 MCS were recorded for $L=20$ at each point. Note that U_F (as well as U_1, U_{DO_3}) must converge to $\frac{2}{3}$ in the respective ordered region, which is borne out nicely by the data and to zero in the disordered region, but should not become negative. The slightly negative values for $L=20$ in (a) at small fields indicate hence insufficient statistical accuracy.

der [Fig. 7(b)]. The data on the size dependence of our order parameters $\langle\,|\psi_1|\,\rangle$ [e.g., Fig. 6(c)] and $\langle\,|M|\,\rangle$ are also reasonably consistent with Ising critical behavior (i.e., critical exponents[47] $\beta\approx 0.32$ for the order parameter, $\nu\approx 0.63$ for the correlation length), unlike the cluster-variation method which invariably implies $\beta=\nu=\frac{1}{2}$, since sufficiently close to the transition it reduces to a Landau-type theory. We emphasize, however, that in the present work no real effort has been made too study the critical behavior thoroughly. More interesting than the critical behavior of the $A2$-ferromagnetic–$A2$-paramagnetic transition and the $B2$-$A2$ transition is the transition at the multicritical point where both these transitions meet, and the transition from the DO_3 phase to the $B2$ phase which belongs to the universality class of the XY model with cubic anisotropy, according to the Landau symmetry classification [cf. Eq. (9)]. However, such an analysis of the critical behavior would require about an order of magnitude more effort in CPU time than was available to us and hence this is left to future work. Here we are rather concerned with an overall description of the phase diagram.

We now turn to a discussion of our procedures in the regions of the phase diagram where the transitions are of first order. Typical Monte Carlo data are shown in Figs. 8 and 9. Performing "sweeps" in temperature or field (i.e., changing temperature or field in small enough steps from one run to the next, e.g., $k_B\Delta T/W_{\rm NN}=0.25$ or $\Delta H/W_{\rm NN}=0.1$, taking the last configuration of the previous temperature or field value as starting configuration for the next value), we look for hysteresis loops (comparing heating and cooling runs when T is changed, or runs with decreasing field to runs with increasing field). Of course, such hysteresis is only observed if (i) the system size is large enough to distinguish clearly the separate phases in the transition region, and (ii) the observation time is long enough to equilibrate the system in one phase but at the same time short enough that one does not yet observe any jumps from one phase to the other, and (iii) the steps are small enough so that the region where the hysteresis occurs is not missed. We have found that in the present model system the hysteresis region often was rather narrow and we did not observe hysteresis because condition (iii) is violated (step width being too large, e.g., in Fig. 9). Then the first-order transition shows up as two branches of one function which do not smoothly join together. In the transition region, it may be that one observes states slowly relaxing from one branch to the other (e.g., the point at

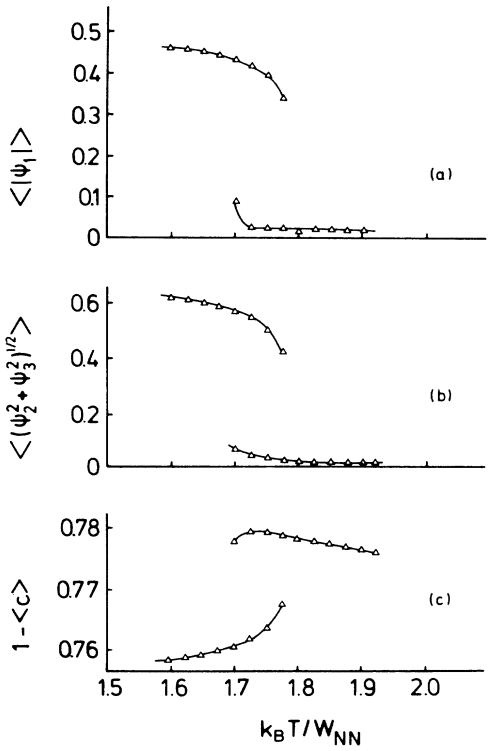

FIG. 8. Temperature variation of the order parameters (a) $\langle\,|\psi_1|\,\rangle$ and (b) $\langle(\psi_2^2+\psi_3^2)^{1/2}\rangle$ and of (c) the concentration at the first-order transition between the paramagnetic DO_3 and paramagnetic $A2$ phase, for $L=20$ and $H/W_{\rm NN}=-9$. Data were generated by "sweeping" the temperature upward or downward, using 500 MCS/site at each data point and the final state of the previous run as a start configuration.

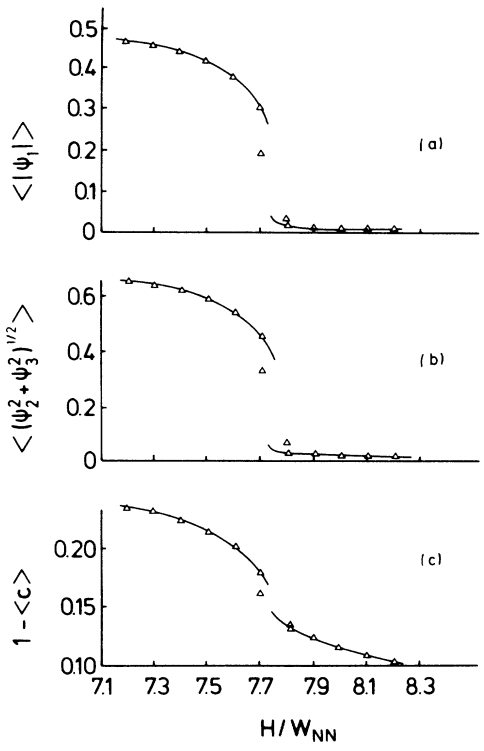

FIG. 9. Variation of the order parameters (a) $\langle\,|\psi_1|\,\rangle$ and (b) $\langle(\psi_2^2+\psi_3^2)^{1/2}\rangle$ and of (c) the concentration with magnetic fields at the first-order transition between the ferromagnetic DO_3 and ferromagnetic $A2$ phase, for $L=20$ and $k_BT/W_{\rm NN}=0.75$. Data were generated by "sweeping" the field upward or downward, using 600 MCS/site for each data point and the final state of the previous run as a start configuration.

$H/W_{NN}=7.7$ obtained by decreasing the field in Fig. 7) which must be disregarded because of their intrinsically kinetic origin.

It is obvious that on the basis of "raw data" such as shown in Figs. 8 and 9 there is some ambiguity in both locating where the transition occurs and estimating the magnitudes of the jumps in the various quantities exhibiting jump singularities as the first-order transition. A first-principles method free from such ambiguities based on finite-size scaling at first-order transitions has recently been suggested and demonstrated to give very reliable results.[48] This method, however, is very time consuming since it requires an accurate sampling of the events where the system jumps from one phase to the other one(s) which compete with it, so that the quasi nonergodicity (which shows up via hysteresis) is completely eliminated. We have not attempted to apply this first-principles method here and thus our phase diagrams in the first-order regions have relatively large error bars (Figs. 12 and 13) because of the ambiguity of locating exactly where the transition occurs (Figs. 8 and 9).

An alternative method of removing this ambiguity is based on estimating the free energy of the various phases and looking for the intersection points of the various free-energy branches. For alloy phase diagrams, the applicability of this method was demonstrated in Ref. 12, and hence we have attempted to apply it here, too. Of course, one has to overcome the standard difficulty of Monte Carlo work that the free energy itself is not an immediate output of a Monte Carlo calculation.[34] While sophisticated methods for estimating F with Monte Carlo techniques have been devised (e.g., Ref. 18), their accuracy in the general case is somewhat uncertain and has to be reinvestigated in every new application; hence we have restricted ourselves to the standard "thermodynamic integration" method.[12] Here we exploit relations such as

$$F=U-TS(T=0)+NT\int_0^T (C/T')dT' \tag{67}$$

and

$$\frac{1}{N}F=4W_{NN}+3W_{NNN}+H-2\int_{-\infty}^{H}\langle c\rangle dH\ . \tag{68}$$

In Eq. (68) the "reference state" with known free energy is the state at $T=0$ [$F=U-TS(T=0)$], in Eq. (68) it is the state for $H\to-\infty$ ($F/N\to 4W_{NN}+3W_{NNN}+H$, $\langle c\rangle\to 0$), and the path integration in Eq. (67) is a path with $H=$const; in Eq. (68) it is a path with $T=$const. Of course, one can consider any other paths in the (H,T) plane which are convenient; often we have considered paths composed of first a piece according to Eqs. (67) and then continuing at constant T according to

$$\frac{1}{N}F=\frac{1}{N}F(T,H_1)-2\int_{H_1}^{H}\langle c\rangle dH+(H-H_1)\ .$$

The application of Eq. (67) requires very accurate specific heats at low temperatures: due to the denominator $1/T'$ small errors δC get magnified. Figure 10 shows, checking the Monte Carlo data with the low-temperature series expansions for C following from Eqs. (19) and (20), that this difficulty is not too serious in practice. Since for many fields the low-temperature series describes the data accurately for $k_BT/W_{NN}\lesssim 0.5$ [e.g., Figs. 10(b) and 10(c)], one can use at very low tempertures directly Eq. (19) as a reference free energy and need not extend Eq. (67) to too low temperatures. One has to be very careful, however, for fields which are very close to the critical fields $H_{c1},\ldots,H_{c4}$, as defined in Eqs. (11)–(15): there C has structure at very low temperatures, as seen both from the series and the Monte Carlo calculation.

Another error in the application of Eqs. (67) and (68) comes from the statistical error of data points as shown in Fig. 10, or Figs. 8(c) and 9(c), and the fact that for the integration one has to fit interpolation curves to these data points. This was done by cubic spline functions. The error associated with these procedures is difficult to estimate; since the resulting free energies cross at very small angle the location of the intersection point is rather sensitive to such an error. We find typically rather accurately defined intersections at low temperatures [Fig. 11(a)], while at intermediate temperatures sweeps with a finer ΔH would be required to locate the intersection point precisely [Fig. 11(b)]; however, at the highest temperatures we sometimes encounter cases [Fig. 11(c)]

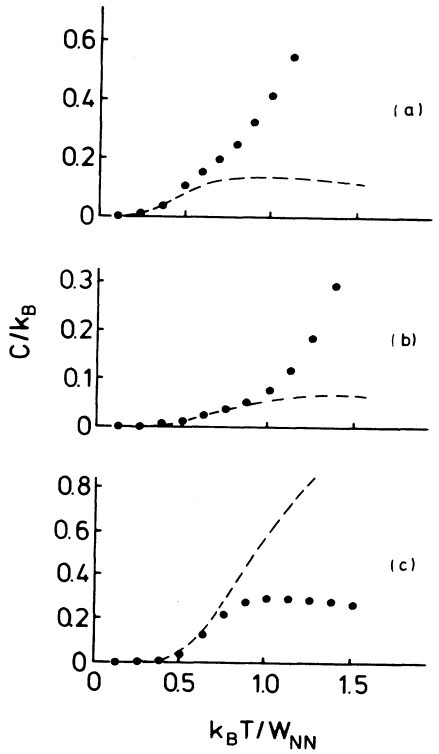

FIG. 10. Temperature variation of the specific heat as obtained from Monte Carlo simulation (dots) and from the low-temperature series expansion (dashed curves). (a) refers to $H/W_{NN}=3.2$ (inside the regime of the ferromagnetic DO_3 phase), (b) refers to $H/W_{NN}=-9.5$ (inside the regime of the paramagnetic DO_3 phase), and (c) refers to $H/W_{NN}=-13$ (inside the regime of the paramagnetic $A2$ phase). All Monte Carlo data were taken with $L=12$ and using 10 000 MCS/site.

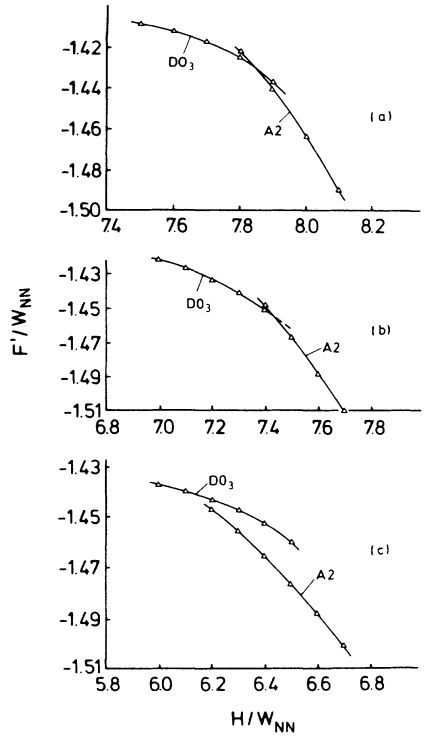

FIG. 11. Variation of free energies of the ferromagnetic DO_3 and ferromagnetic $A2$ phases with field for $k_BT/W_{NN}=0.5$ (a), 1.0 (b), and 1.5 (c). For the sake of clarity of the plot, not the free energy F/N itself, for rather $F/N+\frac{1}{2}H\equiv F'$ is shown. Free energies have been obtained by numerical integration of the specific heat (cf. Fig. 10) and the concentration (Fig. 9) as discussed in the text.

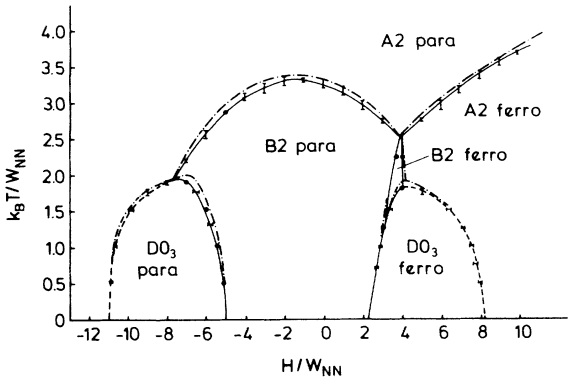

FIG. 12. Comparison of the phase diagram predicted by the cluster-variation method in the tetrahedron approximation (dash-dotted lines) to the phase diagram obtained from the Monte Carlo method, in the grand-canonical ensemble. Nature of the various phases is indicated in the figure. Curves through the Monte Carlo data (shown by error bars or by dots in case the error is smaller than the size of the dot) are guides to the eye only: solid curves denote second-order transitions; dashed curves denote first-order transitions. Note that the error bars may be either horizontal or vertical depending on whether H was varied at constant T or vice versa, in the runs locating the transition line.

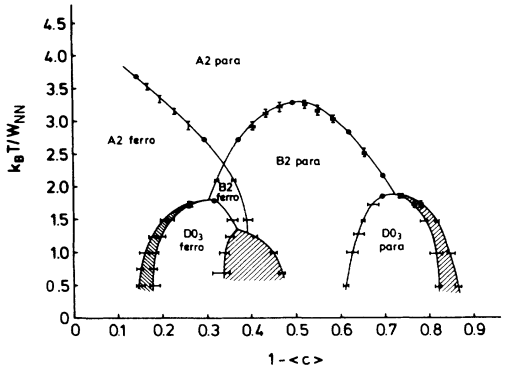

FIG. 13. Same phase diagram as shown in Fig. 12 ($W_{NNN}/W_{NN}=0.5$, $J/W_{NN}=0.7$) but shown in the canonical ensemble rather than the grand-canonical ensemble. Now first-order transitions show up as two-phase regions (shaded). Note that data on transition lines obtained by temperature variation at fixed field now get a horizontal error bar in addition to the vertical one, due to the statistical error of the pseudo spin magnetization (translating into the concentration) at fixed field. Data are shown as dots if error is too small for being resolved. Curves are drawn as guides to the eye only, and the nature of the various phases is indicated.

where the free energies fail to intersect in the region where we know from the direct analysis (such as shown in Figs. 8 and 9) that the transition *must* occur. We attribute this failure to intersect, as shown in Fig. 11(c), to a systematic error in F resulting from the interpolation procedure. Of course, one could do much better taking many more "raw data" points; we have not done so, since even with rather conservative error estimates in the phase diagram (Figs. 12 and 13) its structure is already quite clear.

Figure 12 compares the phase diagram obtained in the grand-canonical ensemble to the phase diagram obtained from the cluster-variation tetrahedron approximation. It is seen that the latter yields the qualitative features of the phase diagram correctly (the phase diagram "topology" is the same, the order of the transitions is predicted correctly). Also in quantitative respect, the transition temperatures are predicted rather accurately: Typically

TABLE I. Some transition temperatures of the phase diagram in the grand-canonical ensemble (CV denotes cluster-variation method; MC the Monte Carlo method).

Field	k_BT_C/W_{NN}		
(H/W_{NN})	CV	MC	$\Delta T_C/T_C$
10	3.7597	3.6750±0.0125	~2.3%
5	2.8208	2.74 ±0.01	~3.0%
4	1.9010	1.793 ±0.007	~6.0%
3	2.8363	2.732 ±0.012	~3.8%
−1	3.3726	3.29 ±0.01	~2.5%
−5	2.9550	2.845 ±0.01	~3.8%
−7	2.2963	2.175 ±0.015	~5.5%
−7	1.9970	1.88 ±0.1	~6.2%

the CV method predicts transition temperatures that are 3% too high; see Table I (somewhat larger errors are encountered only for cases where the transition lines are nearly parallel to the temperature axis). Also in the canonical ensemble the predicted phase diagrams (Figs. 5 and 13) deviate from each other only very little. We conclude that for the present model the cluster-variation tetrahedron approximation yields an unexpectedly reliable prediction for the phase diagram.

VI. CONCLUSION

In this paper we have analyzed the phase diagram of bcc lattice models for binary alloy AB, where one species (A) is magnetic while the other species (B) is nonmagnetic. The interactions are chosen such that at low temperatures the model exhibits both ferromagnetic and paramagnetic crystallographic superstructures of both the $B2$ and DO_3 type, in addition to the ferromagnetic $A2$ phase which occurs as the low-temperature state on the A-rich side of the phase diagram.

This model may be considered as a first step toward the modeling of real alloys such as the Fe-Al system. Unlike Ref. 32, we have not made an attempt to construct interaction parameters such that the phase diagram of the model fits the experimental one for this alloy; a realistic description of this alloy must take the itinerant character of the electrons responsible for the Fe magnetic moments more seriously.[49] Rather, we are concerned with a critical comparison of several current methods for the calculation of phase diagrams of model systems: the Bragg-Williams approximation, the cluster-variation method (in the tetrahedron approximation), and the Monte Carlo method. We find that the Bragg-Williams approximation is seriously in error: it yields several features of the phase diagram which are qualitatively incorrect and overestimates many transition temperatures by about 50% in the model studied numerically. We believe that for other parameter values the failure of the Bragg-Williams approximation will be similarly severe. This is a further reason why the fit to the Fe-Al system obtained in Ref. 32, based on the Bragg-Williams approximation, is not a valid determination of effective interaction energy parameters. In contrast, the accuracy of the cluster-variation calculation is rather good, typically the transition temperatures are overestimated by 3% only (taking the Monte Carlo estimates as reliable estimates for the exact ones). This accuracy of the cluster-variation method is even distinctly better than in similar comparisons for the fcc lattice (discussed in Refs. 2 and 3). This close agreement gives further credence to the suggestion[2,3] that the rather large discrepancies occurring in the case of the fcc lattice with nearest-neighbor interactions only are a consequence of the fact that this lattice is "fully frustrated"[27] which is disadvantageous, a rather exceptional case and not characteristic for most lattice models of practical interest. The reliability of the cluster-variation method for the present model is considered as rather nontrivial, since we have to deal with many distinct phases, three tricritical points, one tetracritical point, and three critical end points occur, and some phase boundaries are rather close together in the phase diagram.

A phenomenon which might be rather interesting also for experimental studies on real alloys (such as Fe_3Al) is the finding that the crystallographic order induces also a staggered magnetization in the ferromagnetic state as a secondary order parameter. Since the squares of the order parameters are proportional to the Bragg intensities of the appropriate Bragg spots in the Brillouin zone, it is implied that the neutron diffraction superlattice Bragg spots of the ferromagnetic DO_3 or $B2$ phases have a magnetic contribution due to this staggered magnetization. This magnetic contribution can be isolated by appropriate magnetic neutron scattering techniques. This staggered magnetization is found already on the level of the Bragg-Williams molecular-field approximation.

From the present work, it should also be evident that for complicated models such as the present one the cluster-variation method requires both some analytical effort [to construct the entropy expression, Eq. (55) in our case] and a nontrivial numerical work (solution of the "natural iteration" equations, diagonalization of the rather huge Hessian matrix, etc.). Although the Monte Carlo method requires a factor 10–100 more CPU time to yield a more reliable phase diagram, as done here, it has a number of distinct advantages. (i) No analytical work at all is required. (ii) Change of the model (different spin quantum number, or choice of classical XY or Heisenberg spins instead of Ising spins, addition of larger-range interactions, etc.) is straightforward. (iii) Reliable results at very low temperatures are easily obtained (see, e.g., Fig. 10). (iv) It is possible to study also the non-Landau-like critical behavior near the second-order transitions, including the multicritical points. Such a study, as well as the generalization mentioned under (ii), are left to future work, however. What is also left to be done is to vary the parameters $W_{\mathrm{NNN}}/W_{\mathrm{NN}}$ and J/W_{NN} systematically [which presently were held fixed in our numerical calculation; see Eq. (48)].

ACKNOWLEDGMENTS

We have profited from stimulating discussions with G. Inden, R. Kikuchi, and D. C. Mattis.

[1]D. de Fontaine, in *Solid State Physics*, edited by H. Ehrenreich, F. Seitz, and D. Turnbull (Academic, New York, 1979), Vol. 34, p. 73.

[2]T. Mohri, J. M. Sanchez, and D. de Fontaine, Acta Metall. **33**, 1171 (1985).

[3]K. Binder, in *Festkörperprobleme (Advances in Solid State Physics)*, edited by P. Grosse (Vieweg, Braunschweig, 1986), Vol. 26, p. 133.

[4]W. Shockley, J. Chem. Phys. **6**, 130 (1938).

[5]J. Büth and G. Inden, Acta. Metall. **30**, 213 (1982); U. Gahn,

Z. Metallkde. **64**, 268 (1973); **65**, 418 (1974); **65**, 735 (1974); Phys. Status Solidi A **29**, 529 (1975).
[6]Y. Y. Li, J. Chem. Phys. **17**, 449 (1949).
[7]R. Kikuchi, J. Chem. Phys. **60**, 1071 (1974); N. S. Golosov, L. E. Popov, and L. Y. Pudan, J. Phys. Chem. Solids **34**, 1149 (1973); **34**, 1159 (1973); C. M. van Baal, Physica **64**, 571 (1973).
[8]J. M. Sanchez, D. de Fontaine, and W. Teitler, Phys. Rev. B **26**, 1465 (1982).
[9]A. Finel and F. Ducastelle, Europhys. Lett. **1**, 135 (1986).
[10]K. Binder, Phys. Rev. Lett. **45**, 811 (1980).
[11]K. Binder, J. L. Lebowitz, M. K. Phani, and M. H. Kalos, Acta Metall. **29**, 1655 (1981).
[12]K. Binder, Z. Phys. B **45**, 61 (1981).
[13]U. Gahn, J. Phys. Chem. Solids **43**, 977 (1982).
[14]H. Ackermann, S. Crusius, and G. Inden, Acta Metall. **34**, 2311 (1986).
[15]U. Gahn, J. Phys. Chem. Solids **47**, 1153 (1986).
[16]H. T. Diep, A. Ghazali, B. Berge, and P. Lallemand, Europhys. Lett. **2**, 603 (1986).
[17]T. L. Polgreen, Phys. Rev. B **29**, 1468 (1984).
[18]H. Meirovitch, Phys. Rev. B **30**, 2866 (1984).
[19]J. M. Sanchez and D. de Fontaine, Phys. Rev. B **21**, 216 (1980); **25**, 1759 (1982).
[20]M. K. Phani, J. L. Lebowitz, and M. H. Kalos, Phys. Rev. B **21**, 4027 (1980).
[21]K. Binder, W. Kinzel, and W. Selke, J. Magn. Magn. Mater. **31-34**, 1145 (1983).
[22]R. A. Bond and D. K. Ross, J. Phys. F **12**, 597 (1982).
[23]J. L. Lebowitz, M. K. Phani, and D. F. Styer, J. Stat. Phys. **38**, 413 (1985).
[24]D. de Fontaine and R. Kikuchi, in *Applications of Phase Diagrams in Metallurgy and Ceramics,* Natl. Bur. Stand. Spec. Publ. No. 496 (U.S. GPO, Washington, D.C., 1978), Vol. 2, p. 976.
[25]D. F. Styer, M. K. Phani, and J. L. Lebowitz, Phys. Rev. B **34**, 3361 (1986).
[26]R. Kikuchi, Phys. Rev. **81**, 998 (1951).
[27]G. Toulouse, Commun. Phys. **2**, 115 (1977).
[28]S. Katsura and S. Fujimori, J. Phys. C **7**, 2506 (1974); G. Inden, Acta Metall. **22**, 945 (1974).
[29]R. Kikuchi and C. M. van Baal, Scr. Metall. **8**, 425 (1974).
[30]D. P. Landau, Phys. Rev. B **16**, 4164 (1976).
[31]C. R. Houska, J. Phys. Chem. Solids **24**, 95 (1963); G. Schlatte, G. Inden, and W. Pitsch, Z. Metallkde. **65**, 94 (1974).
[32]S. V. Semenovskaya, Phys. Status Solidi B **64**, 291 (1974).
[33]P. R. Swann, W. R. Duff, and R. M. Fisher, Metall. Trans. **3**, 409 (1972); S. M. Allen and J. W. Cahn, Acta. Metall. **23**, 1017 (1975); **24**, 425 (1976).
[34]*Monte Carlo Methods in Statistical Physics,* edited by K. Binder (Springer, Berlin, 1986); *Applications of the Monte Carlo Method in Statistical Physics* (Springer, Berlin, 1984).
[35]J. Kanamori, Prog. Theor. Phys. **35**, 16 (1966).
[36]B. Dünweg, Diplomarbeit, Johannes-Gutenberg-Universität Mainz, 1986 (unpublished).
[37]L. D. Landau and E. M. Lifshitz, *Statistical Physics* (Pergamon, London, 1959).
[38]We are indebted to D. C. Mattis for pointing this out to us.
[39]T. Morita, J. Phys. Soc. Jpn. **12**, 753 (1957).
[40]J. Hijmans and J. de Boer, Physica **21**, 471 (1955); **21**, 485 (1955); **21**, 499 (1955).
[41]A. G. Schlijper, Phys. Rev. B **27**, 6841 (1983).
[42]C. E. Dahmani, M. C. Cadeville, J. M. Sanchez, and J. L. Moran-Lopez, Phys. Rev. Lett. **55**, 1208 (1985); J. M. Sanchez and C. Lin, Phys. Rev. B **30**, 1448 (1984); these two papers study the interplay of chemical and magnetic order on the fcc lattice by the CV approximation. See also, F. J. Martinez-Herrera, F. Mejia-Lira, F. Aguilera-Granja, and J. L. Moran-Lopez, Phys. Rev. B **31**, 1686 (1985), where the interplay of magnetic and chemical order in Fe-Co alloys is studied by means of the Bethe approximation.
[43]R. Kikuchi and H. Sato, Acta. Metall. **22**, 1099 (1974); see also, R. Kikuchi (unpublished).
[44]K. Binder, J. Computat. Phys. **59**, 1 (1985).
[45]For $L=20$ one such run needs about 25 min CPU time on the Siemens-Fujitsu VP-100 computer, using a vectorizing program.
[46]One such run takes about 8 min at a Honeywell Bull PDS8 computer and hence is comparable in CPU effort to the CV method.
[47]J. C. le Guillou and J. Zinn-Justin, Phys. Rev. B **21**, 3976 (1980).
[48]K. Binder and D. P. Landau, Phys. Rev. B **30**, 1477 (1984); M. S. S. Challa, D. P. Landau, and K. Binder, *ibid.* B **34**, 1841 (1986).
[49]A crude approximation which perhaps captures some of the essential effects is to work with Ising spins whose magnetic moments depend on the local environment of the lattice; see G. S. Grest, Phys. Rev. B **21**, 165 (1980), where the spin-glass behavior of $Fe_{1-x}Al_x$ alloys at very low temperatures was modeled.